12-2005

Bench Scale Evaluation of Dense Ceramic Membranes for Production of High Purity Hydrogen from Gasification

Binay Kumar Singh
University of Tennessee - Knoxville

To the Graduate Council:

I am submitting herewith a thesis written by Binay Kumar Singh entitled "Bench Scale Evaluation of Dense Ceramic Membranes for Production of High Purity Hydrogen from Gasification." I have examined the final electronic copy of this thesis for form and content and recommend that it be accepted in partial fulfillment of the requirements for the degree of Master of Science, with a major in Chemical Engineering.

Dr. Atul C. Sheth, Major Professor

We have read this thesis and recommend its acceptance:

Dr. Narendra B. Dahotre, Dr. Roy Schulz

Accepted for the Council:
Carolyn R. Hodges

Vice Provost and Dean of the Graduate School

(Original signatures are on file with official student records.)

To the Graduate Council:

I am submitting herewith a thesis written by Binay Kumar Singh entitled "Bench Scale Evaluation of Dense Ceramic Membranes for Production of High Purity Hydrogen from Gasification." I have examined the final electronic copy of this thesis for form and content and recommend that it be accepted in partial fulfillment of the requirements for the degree of Master of Science, with a major in Chemical Engineering.

Dr. Atul C. Sheth

Major Professor

We have read this thesis
and recommend its acceptance:

Dr. Narendra B. Dahotre

Dr. Roy Schulz

Accepted for the Council:

Anne Mayhew

Vice Chancellor and Dean of Graduate Studies

(Original signatures are on file with official student records)

Bench Scale Evaluation of Dense Ceramic Membranes for Production of High Purity Hydrogen from Gasification

A Thesis
Presented for the
Master of Science Degree
The University of Tennessee, Knoxville

Binay Kumar Singh
December 2005

DEDICATION

This thesis is dedicated to my

Mother

ACKNOWLEDGMENT

I would like to express deep gratitude towards my major advisor Dr. Atul C. Sheth. His insightful guidance during research allowed me to grow professionally and develop my abilities as student and a professional. His patience was very helpful in transition from industry to academia. I would also like to express my sincere thanks to Dr. Narendra B. Dahotre for his guidance and help throughout my work, and for serving as a member of the committee. I would also like to thank Dr. Roy Schulz, who served on my Masters' thesis committee, for his valuable suggestions which gave me a better insight into my work.

I am thankful to Mr. Fred Schwartz, Mr. Newton Wright and Mr. Doug Warnberg who helped me in the laser processing of samples, Ms. Kate Lansford who helped and guided me in the microscopy lab. I thank Jim Goodman and Keith Walker for their help in designing and building the experimental setup used in the current work. I also thank Ifeyinwa Oranugo for her help in carrying out the experiments.

I thank Mr. Bob Metgud of Metcon Industries for the financial support under the DOE sponsored SBIR phase I grant (P.O.# 2395-RD101). I also thank Dr Balkrishnan and his staff at Ceramatec Inc. for providing samples of membranes for the experiment and for technical support.

I would like to convey my thanks to my friends Abraham, Nagini, Sricharan and Subhashini for their support during my memorable stay at UTSI.

ABSTRACT

Gasification for production of hydrogen and other useful gases, has achieved increasing importance in recent years. The reactions involved in gasification are favored at high temperatures and they are also limited by thermodynamic equilibrium. The development of membranes which can separate these gases under gasifier exit gas condition will significantly improve process efficiency and economics and simultaneously provide for the recovery of valuable gases. The availability of a membrane with adequate hydrogen selectivity and good thermal and mechanical stability is the key for the successful application of membrane technology in hydrogen production and separation. This work introduces a special method of laser based deposition to synthesize Palladium-Platinum (Pd/Pt)-ceramic composite membranes and permeation results of a ceramic membrane, permeable only to hydrogen, provided by Ceramatec Inc. Thin film Pd was deposited on a ceramic substrate by Nd-YAG laser irradiation of $PdCl_2$ coated on γ-alumina substrate. Similarly a Pt thin film was also synthesized from $PtCl_4$ coated γ-alumina substrate. The parameters of the laser beam were optimized, and a new procedure to synthesize metal-ceramic composite membranes was developed. The characteristics of Pd and Pt coated γ-alumina membranes were studied and compared. Hydrogen permeation experiments were performed in a $CO+CO_2+CH_4+H_2$ environment under typical catalytic steam gasifier exit conditions. The Pd-ceramic composite showed good mechanical and thermal stability with a hydrogen permeability flux of 0.061 (mol/m^2s). The activation energy of the Pd-membrane was found to be 5.39 (kJ/mol) in a temperature range of 900-1300°F. The ceramic membrane provided by Ceramatec Inc. was tested under the same conditions

used to test the Pd membranes. This ceramic membrane showed good thermal and chemical stability and provided the hydrogen permeability flux of 0.0321 (mol/m^2 s).

TABLE OF CONTENTS

LIST OF TABLES

LIST OF FIGURES

LIST OF SYMBOLS

A_i	Gas chromatograph peak area for species *i* in sample gas
$A_{cal,i}$	Gas chromatograph peak area for species *i* in calibration gas
C_H	Hydrogen atom concentration in metal (mol/m^3)
D_M	Diffusion coefficient of hydrogen atom in metal (m^2/s)
d_p	Diameter of pore
e	Magnitude of the electronic charge
E_a	Activation energy (kJ/mol) for hydrogen transport through Pd-membrane
J_{H2}	H_2 flux ($mol/ m^2 s$)
$J_{H2\ (metal)}$	H_2 flux through the metal layer ($mol/ m^2 s$)
$J_{H2\ (pinholes)}$	H_2 flux through the pinholes ($mol/ m^2 s$)
$J_{H2\ (Total)}$	H_2 flux through the metal layer and pinholes ($mol/ m^2 s$)
k’	Hydrogen permeability of metal($mol/(m\ s\ Pa^{0.5})$)
k	Hydrogen permeability of metal($mol/(m\ s\ Pa^n)$)
k_b	Boltzman constant
n	Pressure exponent (0.5-1)
P_{H2}	Hydrogen partial pressure (Pa)
$\mathscr{P}_{H2}$	Hydrogen permeance ($mol/ (m^2\ s\ Pa^n)$)
$P_{H2,\ Perm}$	Partial pressure of hydrogen on permeate side (Pa)
$P_{H2,Ret}$	Partial pressure of hydrogen on retentate side (Pa)
$P_{reactor}$	Total pressure in the reactor (Pa)
R	Gas constant (8.314 J/mol K)

R^2	Coefficient of regression
t	Time (s)
T	Temperature (K)
t_{H+}	Transference numbers of H^+
t_{e-}	Transference numbers of electrons
v	Volumetric flow rate (cc/s)
$y_{CH4,Feed}$	Mole fraction of CH_4 in feed
$y_{CH4,Total}$	Total mole fraction of CH_4 in permeate gases including, from pinhole leakage and from diffusion through metal layer
$y_{H2,Feed}$	Mole fraction of H_2 in feed
$y_{H2,Total}$	Total mole fraction of H_2 in permeate gases including, from pinhole leakage and from diffusion through metal layer
$y_{H2,metal}$	Total mole fraction of H_2 in permeated gases due to diffusion through the metallic layer
X_M	Thickness of membrane (μm)

LIST OF ABBREVIATIONS

CAS	Chemical Abstracts Service
CTE	Coefficient of Thermal Expansion
CVD	Chemical Vapor Deposition
GC	Gas Chromatograph
PVD	Physical Vapor Deposition
TEA	Transversely Excited Atmospheric
TEOS	Tetra-Ethyl-Ortho-Silicate
PVA	Polyvinyl Alcohol
ALTSB	Aluminum-Tri-Sec-Butoxide
M.W.	Molecular Weight
Nd-YAG	Neodymium-Yttrium Aluminum Garnet
kJ	Kilojoules
mol	gram-mole
Pa	Pascal
μ	micro
SEM	Scanning Electron Microscope
UTSI	University of Tennessee Space Institute
XRD	X-Ray Diffraction

1. INTRODUCTION

Background

Sustainable resources will be required to provide many of the world's future energy, food and chemical needs and fossil fuels will continue to play a key role in providing these resources. Out of various fossil fuels, biomass is the one principal sustainable source of food, organic fuels, and organic materials. In the U.S. biomass can provide a domestic and renewable source of carbon containing species for use in transportation, power generation and in the industrial sectors replacing petroleum as the feed stock. Advances in related biotechnology can be used to improve the production and use of renewable biomass resources, thereby positively impacting the economy and the environment. To this end, environmentally friendly technologies are sought that will enable bio-based renewable resources to produce homegrown transportation fuels, chemicals, or consumer products, and generate clean locally-based power. Other fossil fuels such as coal, oil shale etc. can also be used instead of biomass but they are not renewable and their resources will eventually run out.

The U.S. chemical industry faces increasing challenges to balance the demand for continual improvement in energy and environmental performances at the same time maintaining economic viability. Thermo-chemical transformation (or gasification) of hydrocarbon-based mass can be one such option that can impact these challenges and also reduce dependence on foreign, fossil fuel-based feedstock. Usually, the gasification

based technologies involve gasifier followed by a shift reactor and then some kind of separation step. The separation step separates carbon-containing gases from hydrogen to obtain hydrogen-rich gas stream that can be fed to H_2-based fuel cells. In view of CO_2 being perceived as a greenhouse gas, nowadays more emphasis is being placed on development of hydrogen based economy or hydrogen based fuel. Synthesis gas produced from coal or biomass gasification processes contains H_2, N_2, water, CO_2, H_2S and other gases, depending on the particular gasification process. H_2 is an important raw material that has numerous uses in the chemical and fuel industries. Membrane technology must be developed to efficiently separate gases, H_2 from the product under gasifier exit gas conditions, to significantly improve process efficiency and economics and simultaneously provide for the recovery of valuable gases. However, the production of H_2 and the other desirable gases from separate steps of gasification (or thermal transformation) and gas separation will always be limited by the inherent thermodynamic equilibrium established at the given conditions. By combining the chemical reaction and separation steps in a single processing vessel, it will be possible to overcome the limitation established by the process thermodynamics.

Many of the chemical reactions involved in the thermal transformation/gasification are reversible in nature. Some examples are:

$$CH_4 + CO_2 \rightleftarrows 2CO + 2H_2$$

$$CO + H_2O \rightleftarrows H_2 + CO_2$$

$$CO + 3H_2 \rightleftarrows CH_4 + H_2O$$

$$C + CO_2 \rightleftarrows 2CO$$

For such reversible reactions, preferential removal of one or more of the products during reaction will cause a shift in equilibrium, thereby overcoming thermodynamic limitation and pushing the reaction in the desired direction. High temperature membrane can bring about such selective removal of species during reaction, and therefore, reactor incorporating such membrane can be used to increase the reaction yields of desirable products (1). It is claimed that reactors incorporating such membranes perform in-situ separation and offer advantages over conventional fixed bed reactors without built-in membranes in the areas of higher energy efficiency, lower capital and operating costs, compact modular construction, low maintenance cost, and ease of scale up (2). Figure 1, (taken from Ref. 1), shows the increase in methane conversion to CO and H_2 during dry reforming (i.e. reaction with CO_2) in a reactor with a membrane and in fixed bed reactor without membrane. Although the production rate enhancements achieved in this particular case are moderate, the limitations observed in this study can be overcome by incorporating membranes that offer higher selectivity, which will consequently remove only the species of interest with minimal transport of other species.

The idea of reactors incorporating membranes, which seek to combine two distinct functions, i.e. reaction and separation, has been around as a concept since the early stages of membrane technology. However, it has attracted substantial technical interest during the last decade or so. In the early stages of the membrane-based separation field, the

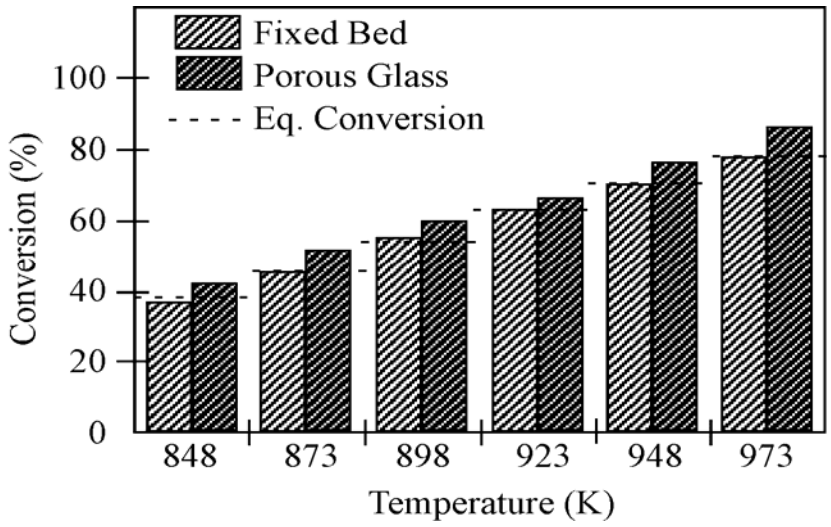

Figure 1 Comparison of methane conversion in a fixed-bed reactor with a membrane (porous glass) reactor (1).

coupling of the two functions was done by simply connecting in series two physically distinct units, the reactor and membrane separator. The concept of membrane-reactors combines two different processing units (i.e., a reactor and a membrane separator) into a single unit. Based on this concept, the purpose of the present study is to develop a ground work for novel gasifier/reactor systems that would incorporate a high temperature membrane to separate gasifier products for production of H_2-rich gas under non-equilibrium conditions.

2. LITERATURE REVIEW

Combining the chemical reaction and separation steps in a single processing vessel has been investigated in several studies. Examples include the dehydrogenation of ethane (3), cyclohexane (4), and ethylbenzene (5); and the hydrogenation of acetylene (6). Uemiya et al. (7) studied the water-gas shift reaction using a palladium membrane reactor in which the product hydrogen permeated the membrane to provide CO conversions in excess of those associated with the "normal" equilibrium conversion. Some of the early studies on membrane reactor applications used noble metal membranes for several hydrogenation and dehydrogenation reactions, and high conversions together with good selectivity were reported (8). Grayaznov et al. (9) used a silver membrane in the oxidation of ethanol and a 50% improvement over equilibrium was obtained. More recently, considerable work has been done with ceramic membranes. H_2S decomposition studies were conducted in a porous-glass membrane reactor by Kamayema et al. (10, 11) who succeeded in selective separation of H_2 from the reacting mixture and reported conversions twice as high as possible from thermodynamic equilibrium. The dehydrogenation of cyclohexane in reactors using platinum impregnated Vycor (12), palladium (tube) (13), and porous glass (14) membranes resulted in conversions 2.5-5 times higher than equilibrium conversion. The dehydrogenation of methanol and *n*-butane was studied by Zaspalis et al.(15) in alumina membrane reactors and a 50% increase in conversions were obtained in the membrane mode of operation as compared to the fixed-bed mode of operation without the membrane. The methane steam reforming reaction was studied by Chai et al. (16) in metal dispersed alumina membrane reactors and conversions twice as high as

thermodynamic equilibrium were reported. The same reaction, studied by Tsotsis et al. (17) in an alumina membrane reactor provided conversions 20% higher than the thermodynamic equilibrium level.

Membrane-based separation processes are today finding widespread and ever increasing use in the petrochemical, food and pharmaceutical industries, in biotechnology, and in a variety of environmental applications, including the treatment of contaminated air and water streams (18). The most direct advantage of a membrane separation process, over more conventional separation counterparts (adsorption, absorption, distillation, etc.), are reported to be in energy saving, and in reduction of the required initial capital investment.

A membrane is a permeable or semi-permeable phase, often in the form of a thin film on a base material. Membranes are made from a variety of materials ranging from inorganic solids to different types of polymers. The main role of the membrane film is to control the exchange of materials between two adjacent fluids phases. For this role, the membrane must be able to act as a barrier, which separates different species either by sieving or by controlling their relative rate of transport through itself. The transport of species across the membrane is the result of a driving force, which is typically associated with the gradient of concentration, pressure, temperature, electric potential, etc. The ability of a membrane to effect separation of mixtures is determined by two parameters, its permeability and selectivity. The permeability is defined as the flux through the membrane divided by the membrane thickness and the driving force. Often the true

membrane thickness is not known and permeance, which is defined as the flux through the membrane divided by the membrane area and the driving force, is utilized instead. The second parameter, called membrane selectivity, $\alpha^{*}_{i,j}$, characterizes ability of the membrane to separates two given molecular species i and j, and which is typically defined as the ratio of either the individual permeabilities or permeances for the two species.

$$\text{Permeance}(\mathcal{P}) = \frac{\text{Moles of gas permeated per unit time}}{\text{(Membrane Area) (Driving Force)}}$$

$$\text{Selectivity}(\alpha^{*}_{i,j}) = \frac{\text{Permeance of component i}}{\text{Permeance of component j}}$$

Broadly, membranes can be categorized as organic (polymeric) membranes and inorganic membranes. Although polymeric membranes exhibit satisfactory permeability and selectivity combined with low cost and easiness in preparation, poor chemical and thermal stability restrict their usages (18). In addition to strong chemical and thermal stability, inorganic membranes exhibit several advantages over polymeric membranes, such as better mechanical strength, freedom from aging, potential to obtain desired catalytic and electrochemical activity, and easiness of tailoring, etc. However, the listed advantages are more than offset by their disadvantages of brittleness and complicated sealing schemes.

According to their structure, inorganic membranes can be divided into two categories, porous inorganic membranes and dense inorganic membranes. Further, they can be categorized into the following three groups (19):

(1) Mesoporous membranes ($2< d_p < 50$ nm), such as alumina, titania and zirconia membranes. The hydrogen permeability of membranes in this group is based on the Knudsen diffusion mechanism. The permeation flux is related to the molecular weight of the diffusing gas. The gas separation selectivity is rather low.

(2) Microporous membranes ($d_p < 2$ nm), such as silica, carbon and zeolite membranes. The pores of membranes in this group are rather smaller in comparison with the first group (by several nanometers). Therefore, the diffusion of hydrogen through these pores is very slow which gives lower permeation flux while selectivity increases significantly.

(3) Dense membranes, such as silica, titania, platinum, palladium and palladium alloy membranes. The mechanism of hydrogen permeation in this group is based on the surface reaction (molecular dissociation) and transport in the form of atoms or ions, which is totally different from that in the first two groups. This mechanism makes selectivity of hydrogen separation very high.

Some typical gas permeation properties of these membranes for hydrogen separation are summarized in Table 1.

Table 1 Typical gas permeation properties of membranes for hydrogen separation

Support	Preparation Method	H_2 Permeance (10^{-8} mol m^{-2} s^{-1} Pa^{-1})	Reference
Vycor	$SiCl_4 + H_2O$ (alternating reactant vapor deposition)	2.2 at 873 K	20
Alumina	Silica (CVD and Sol-gel)	5.4 at 500K	21
α-Alumina Tube	CVD of TEOS by evacuation	4 at 873K	22
Modified Vycor (Nanosil)	High temperature atmospheric CVD of TEOS	1.8 at 873K	1

Membrane technology plays a very important role in hydrogen separation. Since the introduction of polysulfone fiber membranes, used in applications like the recovery of H_2 from ammonia purge gas and extraction of H_2 from petroleum cracking streams (23), there exists a considerable interest in the development of high-performance membranes for hydrogen-separation. Such membranes have the potential for profound improvements in efficiency for separation and purification of hydrogen in applications ranging from gasification to fuels refining. For example, substantial advantages can be gained in operating the water-gas shift reaction at very high temperatures provided that the low equilibrium conversion of carbon monoxide can be enhanced by removing a hydrogen permeate stream through use of a membrane reactor(13, 24, 25) . One particularly significant technical challenge is the development of hydrogen-separation membranes

that can withstand severe operating conditions of temperatures up to 1300°F, and hydrogen pressures up to 300 psi. These conditions are typical of catalytic steam gasification process.

For separation of hydrogen an appropriate inorganic membrane can be used for in-situ separation of hydrogen at elevated temperature without reducing the feed stream temperature. The key factor is the availability of a membrane with adequate hydrogen selectivity and good thermal and mechanical stability. Pd-based composite membranes are expected to possess high thermal and mechanical stability and have sufficient hydrogen permeability and 100% hydrogen selectivity due to the unique property of hydrogen solubility in palladium and the solution-diffusion mechanism for hydrogen permeation through palladium (26). Consequently, palladium-based membranes have received considerable attention for high temperature reaction and separation applications. The hydrogen permeability of palladium membranes is inversely proportional to the membrane thickness while the hydrogen selectivity is highly dependent on obtaining a dense structure in a thin palladium film. Therefore, a viable palladium membrane for high temperature reaction and separation should be a thin, defect-free, composite membrane.

Palladium is an attractive membrane material due to its ability to readily dissociate molecular hydrogen at its surface. Table 2 shows hydrogen permeance for some metal at 560°C. Although some other metals, such as zirconium, niobium, tantalum and vanadium, exhibit significantly higher bulk hydrogen permeability, these metals form oxide layers by surface reaction limiting the hydrogen flux. Hydrogen embrittlement of

Table 2 Hydrogen permeance for some metals at 560°C

Metal	Hydrogen permeance (mol/m.sPa$^{0.5}$)
Niobium	6×10^{-7}
Vanadium	2×10^{-7}
Tantalum	1×10^{-7}
Palladium	4×10^{-8}
Iron	5×10^{-10}
Platinum	6×10^{-12}

these metals is also a reason for their less use for hydrogen separation. As a result, the direct replacement of palladium by cheaper refractory metals is sought for (27). Since palladium is a precious metal, its efficient economic use for industrial applications makes it necessary to reduce the material costs by decreasing the thickness of palladium films. Meanwhile, the reduced thickness would result in higher hydrogen flux without compromising selectivity for hydrogen over other gases. The most significant improvement would be the development of new multilayer membranes consisting of at least two layers. An ultra thin palladium layer combined with a porous ceramic, where the microporous base provides the necessary mechanical support to the thin metallic layer. Platinum can also be considered as suitable replacement for palladium.

Dense inorganic membranes consist of solid layers of metals, such as Pd, Pt, Pd/Ag alloys, or solid oxides (such as ionic conductors). In order to increase the effectiveness of permeability, especially to reduce the critical membrane thickness, the membranes are

applied in the form of multi-layers. The thin dense inorganic membranes usually consist of dense top layers supported on porous ceramic base material. The multi-layer membranes generally have different morphologies with a gradual decrease in the pore size of each layer so that good continuity and adhesion between layers can be achieved. The pore size of these membranes depends on the particle size and the methods by which they are prepared. Ceramic membranes are asymmetric layered structures composed of a separation layer which fulfills the actual membrane function, and a ceramic support structure comprising 1 to 5 layers (3, 17). The support structure which serves as a substrate is needed for general mechanical stability and must have larger pores than the separation layer to reduce the resistance to the desired species flux.

In considering support requirements, the following factors are most relevant to the process:

1. The thermal expansion behaviour of the coating in comparison with the substrate.
2. The substrate/membrane interaction (physical or chemical)
3. The chemical compatibility between substrate material and membrane material.

There must be sufficient sintering or chemical bonding or interlocking of the membrane material with the substrate to ensure proper adhesion of the membrane to the support during application. If the chemical composition of the membrane differs from that of the substrate intermediate layers may be needed. Reasons for applying intermediate layers between the top layer and membrane layer are:

1. Matching thermal expansion, and

2. Providing buffer zone in case of chemical incompatibility during processing.

Alumina (Al_2O_3) is one of the crystalline materials most widely used as support material. Using α–alumina as the support provides the optimum results in terms of activity, mechanical strength and reproducibility. The pore size and smoothness of the surface of the substrate are crucial. The surface pore size should neither be too large to support thin films nor too small to allow free flow of diffusing gas. If the surface is too coarse, formation of a thin film without holes is difficult. Similarly, if surface is too smooth it will prevent adherence of the film with the substrate (28). To get a uniform and smooth surface of the substrate, a γ-alumina layer is first deposited on α-alumina substrate. γ-Alumina has cubic crystal structure which is more open and hence, conducive for flow of hydrogen. The sol-gel method (28) is considered to be the most practical method for depositing γ-alumina layer on α-alumina substrate.

Recently, several studies have been performed on the preparation of such thin supported palladium membranes. The chemical plating method has been successfully used by researchers to coat membrane films of thickness 4-6 μm (29, 30). Though the selectivity of these membranes is good, the process is cumbersome and time consuming. Also, it is not easy to control the thickness of the film as desired and possible decomposition in chemical bath may result in costly losses of palladium. One research group, Shu et al.(31), has studied the physical properties of simultaneously deposited films of palladium and silver coated by electroless plating. Chemical vapor deposition (CVD) has also been used to plug the pores of a ceramic support with palladium (32, 33, 34).

However, due to the high purity and strict deposition conditions required for this process, CVD is not considered to be an economic process. Recently, Li et al. (35) have used the spray pyrolysis technique to successfully coat 2μm thick Pd/Ag alloy membranes. All of the above mentioned processes, aside from the fact that they are time consuming and lack of inexpensive precursors with desired volatility and chemical properties and further, there is always a possibility that unwanted compounds may be formed in the process and incorporated in the Pd membrane as impurities (34). Physical vapor deposition techniques, like sputtering deposition, has better control on film thickness but the rate of deposition is low and efficient cleaning of the surface prior to deposition is very crucial.

At UTSI, a thin (< 1.5 μm) layer of nano-Cerium Oxide (CeO_2) has been successfully deposited on a nickel (Ni) substrate using a pulsed TEA-CO_2 laser (36). Such a direct laser direct fabrication technique should be capable of depositing thin film of Pd or Pt over ceramic support materials. A suitable compound containing Pt and Pd can be applied to a support material and used for such a deposition technique. The compound can then be easily decomposed by laser application to give the required metal layer on the ceramic. The main advantages of this UTSI-pioneered technique, compared to sputtering, physical vapor deposition (PVD) or chemical vapor deposition (CVD) processes, is that no vacuum and/or controlled environment installation is needed and it can be done at atmospheric conditions. The applied laser beam produces large energy fluxes delivered at small location on the substrate which avoids heating the whole substrate and thereby avoids damaging the whole substrate structure, and, at the same time saves substantial energy. Precise control over laser processing parameters could

provide the heat sources necessary to manipulate the thin layer, interface and the region around the interface in the substrate material. The process is well suited for automation; hence large scale and complex structures can be coated with relative ease and high speed. This process can also be used in large volume production at relatively low cost.

The purpose of the present thesis is to report the development of laser-induced-surface-improvement (LISI) method for manufacturing H_2 permeable membranes based on thin films of Pd and Pt on ceramic substrate. The thesis also describes the experimental performance of in-house prepared membranes and a Ceramatec, Inc., provided membrane, in separating hydrogen from simulated gasification process stream.

3. THEORETICAL DISCUSSION

Palladium Membrane

The hydrogen permeation mechanism through a palladium membrane has been studied extensively (26, 27, 28). Hydrogen permeates through metals by a multistep process, which involves the following steps

(1) reversible dissociative chemisorption of molecular hydrogen on the membrane surface,

(2) reversible dissolution of surface atomic hydrogen in the bulk layers of the metal, and

(3) diffusion of atomic hydrogen through the bulk metal.

Figure 2 shows a schematic of the mechanism of hydrogen transport through palladium membrane. Steps 1 and 2 of reversible chemisorption and reversible dissolution take place on both entering (feed side) and exiting (permeate side) surfaces of the Pd membrane.

The ability to transport hydrogen through palladium membranes is typically quantified in terms of permeability, permeance or flux. The flux of hydrogen (J_{H2}) through a palladium layer is the product of the diffusion coefficient (D_M) and the concentration gradient, with the flux of hydrogen atoms (J_H) being twice that of hydrogen molecules:

$$H_2 \rightleftarrows 2H$$

$$J_H = 2J_{H_2} = -D_M \frac{\Delta C_H}{X_M} = D_M \left(\frac{C_{H,\mathrm{Ret}} - C_{H,Perm}}{X_M}\right) \quad (3.1)$$

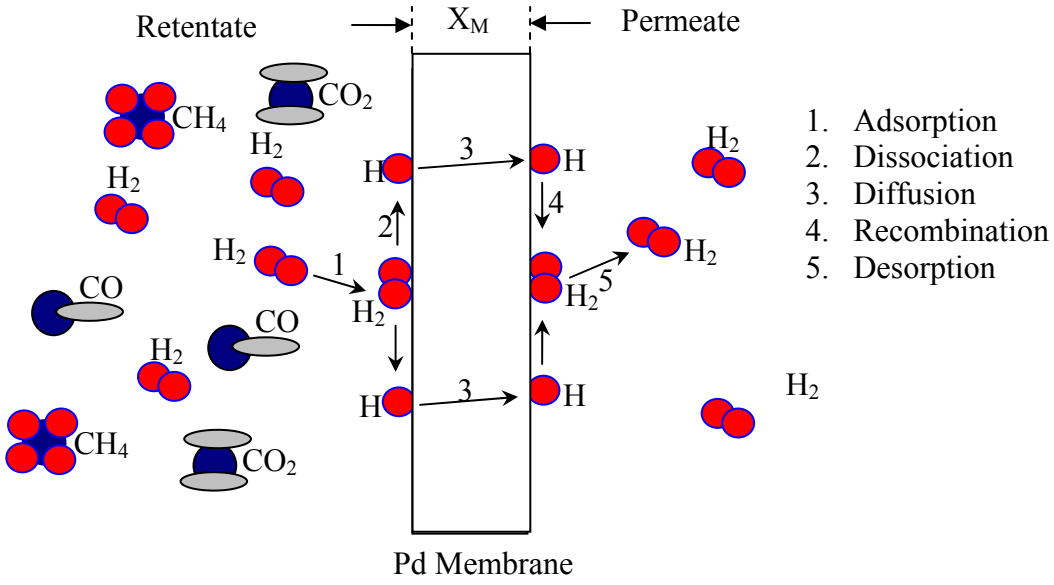

Figure 2 Mechanism of H_2 transport through Pd layer

Where C_H is hydrogen atom concentration in palladium and X_M is the thickness of palladium layer. For thick membranes (X_M > 100 μm), the limiting resistance is assumed to be the transport of hydrogen atoms through the palladium. In the case of thick membranes, the surface reaction is considered to be very fast and the dissolved hydrogen atoms at the surface of the palladium are assumed to be in equilibrium with the hydrogen gas on the respective side of the membrane. The concentration of hydrogen atoms in the palladium can be related to the hydrogen partial pressure via Sievert's equation (37) as shown in Eq 3.2. The exponent of 0.5 reflects the dissociation of the gaseous hydrogen molecule into two hydrogen atoms that diffuse into the metal, where an ideal solution of hydrogen atoms in palladium is formed:

$$K_{eq} = \frac{C_H^2}{C_{H_2}}$$

$$C_H = (K_{eq} C_{H_2})^{0.5}$$

$$C_H = K_{S1} C_{H_2}{}^{0.5}$$

By ideal gas law,

$$C = \frac{P}{RT}$$

Where K_{eq} and K_{S1} are constants and using ideal gas law for relating concentration with pressure we get,

$$C_H = K_S P_{H_2}^{0.5} \qquad (3.2)$$

K_S is the Sievert's constant. Combining these expressions yields the following equation:

$$J_{H_2} = \frac{1}{2} D_M K_S \frac{(P_{H_2,ret}^{0.5} - P_{H_2,perm}^{0.5})}{X_M} \qquad (3.3)$$

The hydrogen permeability of the palladium corresponds to the constants in Eq. (3.3), i.e. one half of the product of the diffusion coefficient and the Sievert's constant:

$$k' = \frac{1}{2} D_M K_S \qquad (3.4)$$

Therefore, the hydrogen flux is inversely proportional to the membrane thickness and directly proportional to the product of the hydrogen permeability and the hydrogen partial pressure gradient across the membrane (37):

$$J_{H_2} = k' \frac{(P_{H_2,ret}^{0.5} - P_{H_2,perm}^{0.5})}{X_M} \qquad (3.5)$$

Most prior investigations of unsupported, bulk palladium membranes (X_M > 100 μm) have been expressed in terms of Eq. 3.5. More generally, an expression for flux can be derived as being proportional to the difference of the hydrogen partial pressure raised to an exponent with a value of 'n', as shown in Eq. 3.6:

$$J_{H_2} = k\frac{(P_{H_2,ret}^n - P_{H_2,perm}^n)}{X_M} \qquad (3.6)$$

Values of 'n' greater than 0.5 are commonly reported in thin supported palladium membrane studies, where it is possible that the validity of the diffusion limited hydrogen transport mechanism assumption is debatable. An exponent value of 0 .5 is indicative of the hydrogen atoms forming an ideal solution in palladium, thus leading to a diffusion limited transport mechanism. Similarly a partial pressure exponent value approaching unity would indicate that a surface adsorption/dissociation or gaseous diffusion type process is the limiting factor. Partial pressure exponent values in the range of 0.5 and 1.0 may be attributable to a combination of a more complex transport mechanism involving both surface effects and the hydrogen diffusion process.

When the value of *n* does not depend on the temperature, the temperature dependence of the gas permeability can be expressed by an Arrhenius equation as

$$k = k_0.\exp\left(-\frac{E_a}{RT}\right) \qquad (3.7)$$

This equation assumes that the value of n in Eq 3.6 does not vary with temperature. In fact, n may also depend on temperature since it is influenced by the solubility and the relative rates of surface processes and bulk diffusion, which all could depend on temperature.

Laser Induced Surface Improvement

Laser induced surface improvement (LISI) is a process where a thin layer at the surface and/or subsurface region of a metal is melted by a laser bean with the simultaneous addition of precursor consisting of water soluble binder/vehicle and powder material of desired element(s). The electro-magnetic radiation of laser beam is absorbed with first few atomic layers for opaque materials, such as metals, ceramics. Typical surface alteration process using lasers traditionally include (i) transformation hardening, (ii) surface melting, (ii) surface cladding, (iv) surface alloying and (v) other techniques (surface smoothening, texturing, coating removal and micromachining) (38). In surface modification techniques, the interaction time between the laser and the substrate is of fundamental importance in determining which of the above mention process will occur. The major independent process variables for the laser modification are laser traverse speed, power, beam shape and size, thermo-physical properties (decomposition temperature, thermal conductivity etc.), thickness and type of pre-coated precursor. By controlling these parameters, depth, width, solute content and microstructure of the laser modified zone can be altered. However, the most important factors among these are power, traverse speed and the diameter of the laser beam. An increase in power increases

the depth irrespective of the level of beam diameter and speed. If the beam diameter is increased with the power and speed being constant, power density decreases at the surface leading to decrease in depth of laser alloyed zone. The width of laser modified zone can be independently controlled by manipulating beam power and speed. This is done by manipulating the amount of energy dumped in the processing area.

A Neodymium doped Yttrium Aluminum Garnet (Nd-YAG) laser which was applied in the present study and CO_2 lasers are mainly used in industrial application because of their high power density. The Nd-YAG laser is a solid state, usually pulsed, flashlight actuated laser. The medium responsible for laser action is neodymium. The Nd-YAG lasers emit radiations of 1.06 μm wavelength.

At the Center for Laser Applications (CLA) at UTSI, extensive work has been done in area of laser surface modification. Surface modification has been performed by alloying, depositing thin layers of borides (39) and carbides (40) on metal like aluminum, aluminum alloys, iron, iron alloys etc. Ceramic coatings (41) have been applied to aluminum alloy substrate, which showed enhanced surface properties such hardness and wear resistance. In coating of iron oxide on aluminum alloy, formation of reaction product in the interface between iron oxide and aluminum matrix ensured good bonding (reaction induced bonding) between the reinforcing ceramic and the matrix. Composite boride coating on plain carbon steel showed minimized temperature oxidation. Surface processing of alumina grinding wheel materials was carried out (42, 43) using laser beam of power ranging from 500-1000 watts.

Modifications of surfaces by laser have various advantages. In the words of Dahotre (44), some of the main advantages are:

- A chemically clean light source delivers precisely controlled energy to localized zone.
- Optical elements or fibers easily maneuvers the beam, and these can be adapted to automation which is suited for automation that is suited for processing in ambient environment of large scale and complex structures with ease and high speed.
- Narrow beams with high power density allow extremely rapid processing, with minimal or no change in the bulk material.
- Rapid rates of processing procedures refined and novel microstructures in the surface region.
- Precision associated with coherent and monochromatic beam combined with automation allows the possibility of near net shape processing with tailored properties.

Ceramatec® Membrane

Ceramatec, Inc. is a research and development company focused on the creation of new products and business in advanced materials and electrochemistry. The membrane provided by Ceramatec Inc. was a dense ceramic membrane. Dense inorganic membranes are referred to as those membranes made of a polycrystalline ceramic or metal, which allows certain gas species to permeate through their crystal lattice (45). Dense ceramic membranes are 100 percent hydrogen selective and are not subject to problems associated

with pore clogging. Ceramic materials developed for this type of membrane are also relatively inexpensive compared to metals such as palladium currently used in the composition of metallic membranes. The transport mechanism in dense ceramic membranes occurs at temperatures compatible with coal/biomass gasification and chemical processes. Hydrogen flux through dense ceramic membranes is usually very low compared to other membrane technologies. Most dense ceramic membranes under development are based on perovskite materials (46). These materials, often composed of barium and strontium cerates, are not chemically stable in coal syngas environments containing high concentrations of CO_2 and steam. Effort is also being placed on the development of pure ceramic materials, which are more mechanically stable than cermet (ceramic-metallic) membranes. These types of dense membranes are proton conducting membranes that selectively transport H^+ ions under driving forces such as a pressure difference or an applied voltage.

In a pressure driven system, both hydrogen ions and electrons generated by dissociation of H_2 molecules at the high pressure surface must be transported through the membrane to recombine at the low pressure surface. Since hydrogen and electron transport are parallel kinetic processes, the overall kinetics are limited by the slowest process. In the case of a conventional mixed conducting single phase membrane, the paths for proton conduction and electron conduction are the same. The proton flux (J_{H+}) through the membrane where the primary charge carrying species are H^+ and e^- can be shown (46) as:

$$J_{H^+} = -\frac{k_b T}{2e^2}\int_i^0 (\sigma t_{H^+} t_{e^-}) d(\ln P_{H_2}) \qquad (3.8)$$

Where k_b is Boltzman constant, T is the absolute temperature in Kelvin, e is the magnitude of the electronic charge, σ is the total electrical conductivity, P_{H2} is the partial pressure of hydrogen and t_{H+} and t_{e-} are the transference numbers of H^+ ions and electrons through the membrane. The hydrogen flux thus depends on having high conductivity of both species. The electronic conductivity of perovskites is very low and is usually the factor limiting the effective use of these materials for pressure driven hydrogen separation. An approach has been applied to separate the conduction paths of H^+ ions and electrons through incorporation of a second phase ceramic, thereby eliminating the combined dependence of hydrogen flux on both electronic and proton conductivities. By short circuiting the electron flow paths the overall flux is limited only by the proton conductivity. In addition to being a good electronic conductor, the material chosen as the second phase should also possess good thermo-mechanical and thermo-chemical stability. Ceramatec® has developed a proprietary ceramic-ceramic composite material in which independent migration paths of proton and electron species occurs through an interpenetrating network of proton and electron conducting ceramic phases.

Sol-gel Method for Preparing Surface Coating

Sols are lyophobic (solvent hating) suspension of solid particles (1 to 1000 nanometres in size) in a liquid. The sol-gel method for preparing surface coating is based on the phase transformation of a sol obtained from metallic alkoxides or organometallic precursors.

The first stage in the sol-gel process consists of the preparation of a sol using molecular precursors, either metal salts or metal organics. In both cases condensation reactions occur at the sol stage with formation of colloids or clusters, which collide at the final stage to form the gel. In the case of membrane formation, it is important to note that coating of the active layer must be carried out at the sol stage with a rheological behavior adapted to the porous substrate chosen as the membrane support. Supported membranes are prepared by a dipping procedure (33). This is called a slip-casting process. According to this method, a capillary pressure drop is created by bringing a microporous ceramic support into contact with a stable sol. A pressure drop due to capillarity forces the dispersion medium of the sol to flow into the dry pores of the support. The sol particles are concentrated at the entrance of the pores and a gel is formed. This gel can be dried and calcined to form a crack free supported membrane. The factors that determine whether or not a gel layer forms during dipping are sol concentration, dipping time, pore size of the support and the type and amount of acid used to peptize the sol. The presence of dust particles as well as a partial gelation in the sol must be avoided in order to prevent the formation of defects and pinholes in the membrane. The drying and sintering steps will determine the nature of the membrane. The advantages of the sol-gel methods are its versatility and the possibility to obtain high purity materials (shaped as monolithic blocks, powders or thin layers) with perfectly controlled compositions. The main disadvantage of the sol-gel membrane is its temperature limitation.

4. EXPERIMENTAL PROCEDURES

Synthesis of γ-Al_2O_3 Membrane

The substrates used were porous alumina membrane discs 20 mm in diameter and about 4 mm thick. The top-layer of the substrate membrane was a 5-7 μm thick γ-Al_2O_3 layer supported on a coarse porous α-alumina substrate (38% porosity, 0.5 μm pore diameter, Coorstek®, item# 60002). One side of each disk was polished with sand papers #320, #500 and #800, successively, and examined visually as well as by optical microscope for defects before coating. The substrates were flushed with nitrogen to remove any dust particle. The presence of dust particles must be avoided in order to prevent the formation of defects and pinholes in the metallic membranes that will be formed on the ceramic surface.

In preparing the supported membranes, 20 ml of 1M boehmite sol (colloid), AlO(OH), was mixed with 13 ml of 3 wt% polyvinyl alcohol (PVA) solution. The α-Al_2O_3 porous supports were dip-coated, on one side only, with the boehmite and PVA mixture. PVA acts as a binder to prevent crack formation during the drying process as well as helping to adjust the sol viscosity (as a thickener). Polyvinyl alcohol not only acts as a colloid stabilizer, it also controls the porosity of the support material without changing its other microstructural properties significantly. It burns off gradually without leaving an ash or tar. The alumina substrates were dipped in boehmite and PVA solution, on one side only, for 8-10 seconds twice in an interval of 2 minutes and third time only for 3 seconds. The

setup shown in Figure 3 was used to carry out the dipping. The excess amount of the solution was wiped off very carefully from the surface with lint guard wipe (Kimberly Clark). Wiping off excess sol is very important because excess solution form a thick layer on certain areas, which tend to crack when calcination is done. Unsupported γ–Al_2O_3 membranes were prepared by drying a small amount of the same boehmite/PVA mixture in petri-dishes. The resulting unsupported membranes were irregularly shaped thin sheets of about 100 μm in thickness. All of the samples were dried in an oven at 40 °C for 2 days in 50% humid air, and then calcined by following temperature program given in Table 3 (47).

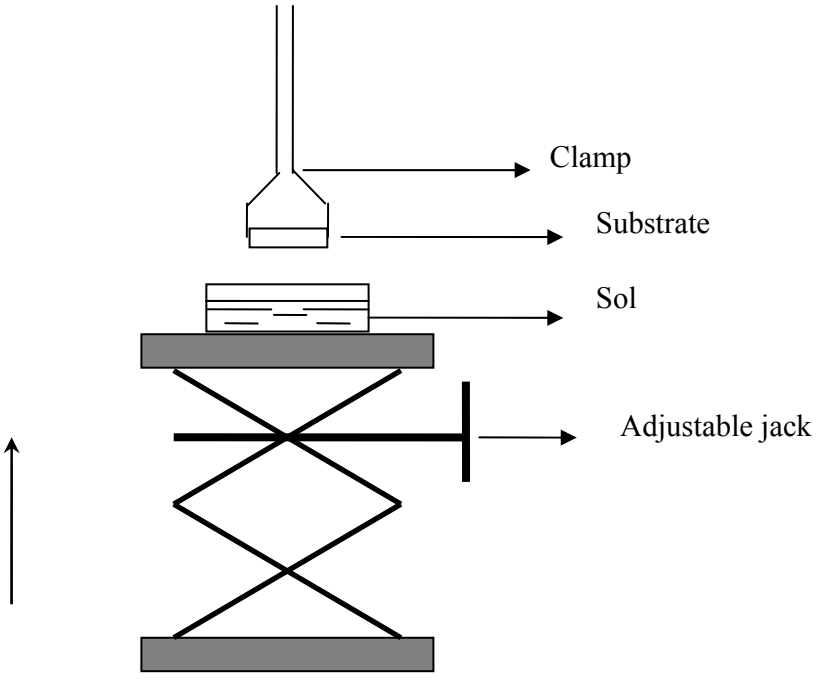

Figure 3 Setup for dip coating of alumina substrate

Table 3 Calcination program for γ-alumina coated alumina

Temperature	Heating Steps
20-450°C	ramped up at@ 30°C/hour
450°C	hold for 3 hours
450-350°C	ramped down at @ 30°C/hour
350°C-room temp.	cool down naturally

Preparation of Boehmite Sol

The preparation of the 1 M boehmite sol first involved heating 100 ml of deionized water in a three neck flask with vigorous stirring. The three-neck flask was placed in an oil bath on a heater and magnetic stirrer plate. One of the necks of the flask had a stopper with a thermometer in it, another neck had a condenser with cold water running through it, and the third neck had a stopper. Next one-tenth mole of aluminum-tri-sec-butoxide was measured out (ALTSB, Alfa Aesar, MW=246.33, 97% purity, 0.1mole ≈ 26 ml) and slowly added to 100 ml of water heated at 70-90°C with a gradual increase in stirring carried out over a period of an hour. After the ALTSB was added the solution was allowed to sit at 70-90°C for one hour to homogenize. Next, 7 ml of 1 M nitric acid was added to the solution while reducing the stirring speed. And finally, the solution was refluxed for ten hours at 90-100°C. The preparation setup used is shown in Figure 4. Preparation of boehmite sol is also discussed in detail by Yoldas (48).

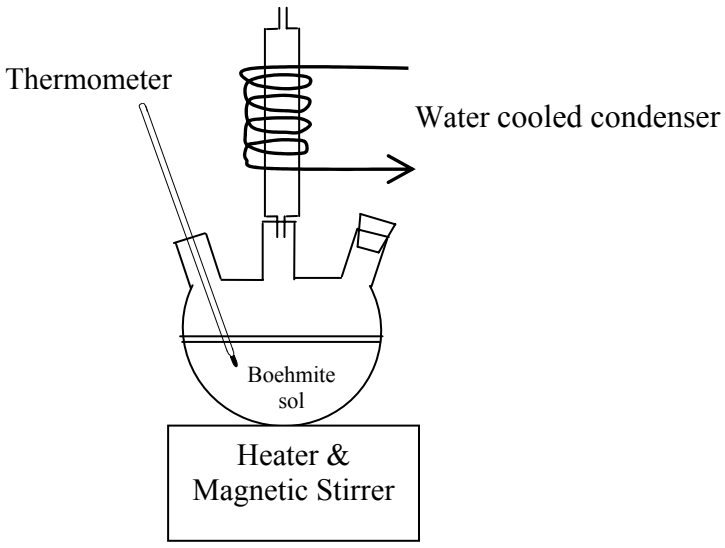

Figure 4 Schematic for Boehmite sol preparation

Preparation of Polyvinyl Alcohol Solution

The preparation of 3 wt % polyvinyl alcohol (PVA) solution involved adding 7.5 grams of PVA (CAS Number: 9002-89-5, 86-89% hydrolyzed, M.W. =60000, Alfa Aesar) very slowly to 250 ml of distilled water at room temperature. PVA was added very slowly to prevent the formation of swelling lumps which are very difficult to completely dissolve. After adding 7.5 grams of PVA, the slurry was continuously stirred for about 10-15 minutes without raising the temperature. This was done in order to disperse the particles efficiently. To shorten the dissolving time, the water temperature was then raised to about 95°C. Partially hydrolyzed PVA is more likely to produce foam, so rapid increases in temperature or stirring were avoided.

Palladium Chloride Layer Deposition

Palladium (II) chloride ($PdCl_2$) layers were deposited on both the α-alumina disc and the γ-alumina disc. Palladium chloride (CAS# 7647-10-1, 99.9%, City Chemicals) was finely crushed and 0.3 grams of it was added to 10 ml of distilled water to make slurry. The polished side of an α-alumina disc was dipped in the palladium chloride slurry for 2 minutes. Then the sample was dried at 100°C for 12 hours before laser processing. This process of dip coating with the palladium chloride slurry did not work with the γ-alumina layer because of its smooth surface. So 0.3 gram of palladium chloride was mixed with 1 ml of water to form thick slurry and using a paint brush a thin and uniform layer was applied on surface of the γ-alumina layer. Then this was also heated to 100°C and held at temperature for 12 hours to dry the sample for laser treatment. The expected dissociation reaction of $PdCl_2$ on laser treatment is given below:

$$PdCl_2 \xrightarrow{675^oC} Pd + Cl_2 \uparrow$$

Platinum Chloride Layer Deposition

Platinum (IV) chloride ($PtCl_4$) layers were deposited on both α-alumina disc and γ-alumina discs. This chemical is hygroscopic and highly soluble in water. It could not be deposited with the same method that palladium chloride was deposited on the α-alumina surface. The reason is that $PtCl_4$ would go deep down into the pores of the substrate and would not form a layer on the top surface. $PtCl_4$ (CAS# 16941-12-1, City Chemicals) was crushed and a solution of 1 gram of it was made in 1 ml of distilled water. By dissolving

platinum chloride in a very small amount of water a thick solution was achieved which did form a layer on the surface of the substrate. Using a paint brush, a thin and uniform layer was prepared on the surface of α-Al_2O_3 and γ-Al_2O_3. These samples were heated to 100°C and held at this temperature for 12 hours. The expected dissociation reaction of $PtCl_4$ on laser treatment is given below:

$$PtCl_4 \xrightarrow{370^{o}C} Pt + 2Cl_2 \uparrow$$

Laser Processing

A 200 watt Hobart HLP 300 continuous wave Nd-YAG (1.06μm) laser equipped with fiber optic beam delivery system was employed for laser treatment of samples. The fiber optic-beam-delivery system consisted of input coupling module, the fiber optic and output-coupling module. The input coupling module focuses the laser output onto the end of the fiber. The optical fiber in the present system is 17 meter long and about 600μm in diameter. The output coupling module is a telescopic tube (6.35 cm diameter) that can be housed with various configurations of cylindrical and concave lenses firstly to collimate and then either to focus or defocus into various shapes of the beam onto the workpiece. The fiber optic beam delivery provided efficient (with only 4-5% loss) laser energy input to work piece. The lenses within the output-coupling module of fiber optic were configured to provide a beam of 3.5 mm wide in spatial distribution onto the sample surface. Such a line beam provides the energy distribution within the beam suitable to maintain minimum or no overlap between the successive laser passes as required to achieve larger surface coverage in the processed region. The laser beam was focused at

0.5 mm above the surface of the substrate using '6864' optics. Figure 5 is a schematic illustration of the laser processing setup.

Metal coatings were produced in air (at atmospheric pressure) at a power level of 200 watts with a laser beam traverse speed of 4000 mm/min. The laser beam was traced in straight, overlapping stripes so that entire surface of the sample was covered. An overlapping index of 1 mm and a working distance of 123 mm were maintained in the processing of all the samples. A computer numeric control system U-500 was used with program "Yraster" to control the laser beam movement on the surface.

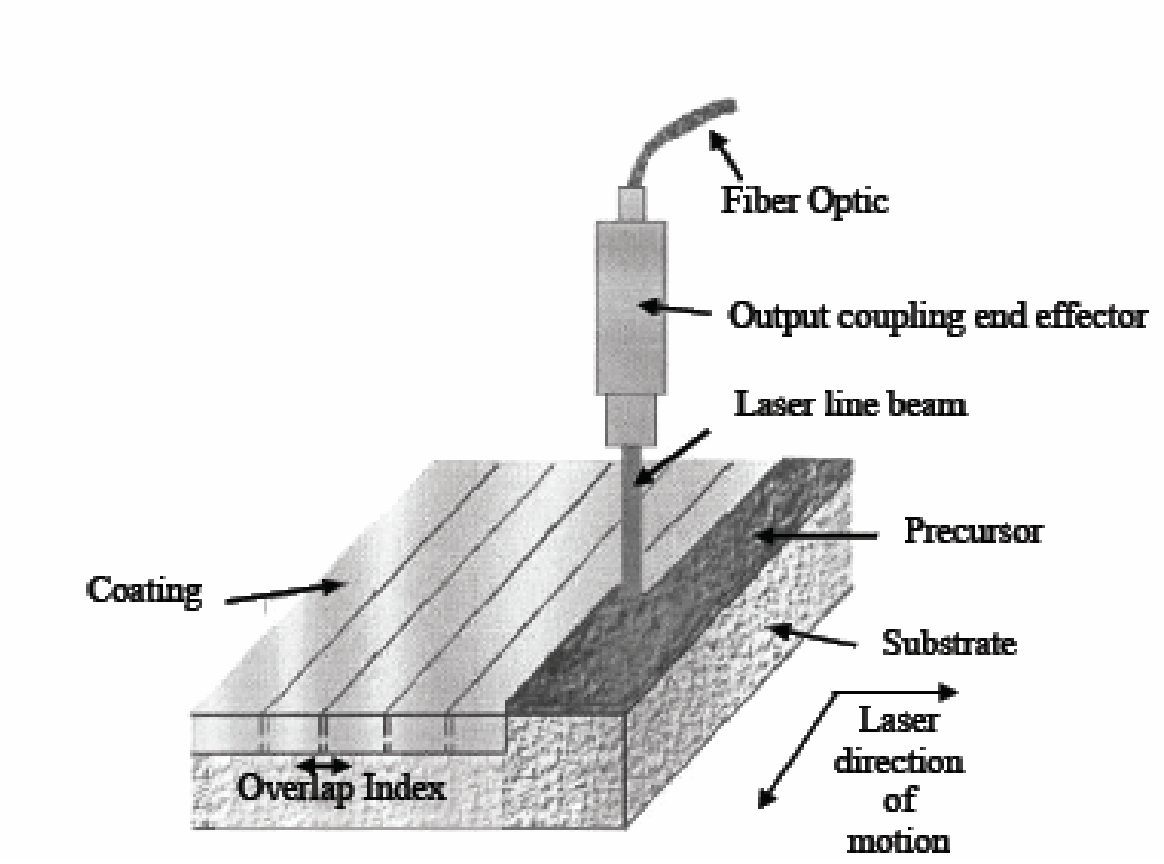

Figure 5 Schematic of laser setup

Hydrogen Permeation

Hydrogen permeation measurements were carried out in a bench scale high-pressure and high-temperature reactor system. A schematic of the hydrogen permeation measurement system is shown in Figure 6. Based on the information provided by Ceramatec Inc., the electrically heated reactor part of this bench scale unit for testing permeability of various membranes was constructed out of a 3 inch type 304 stainless steel tubing, with a wall thickness of 0.0065-inch. This allowed a working pressure as high as 80 psi at 1200°F. K-type thermocouples were introduced from both ends. One thermocouple was used to monitor the temperature in the reactor body and the other to measure temperature near the membrane. Gases were supplied to the reactor from storage cylinders connected through three flowmeters (Dwyer Instruments, Inc.). The flowmeters were used to get desired gas compositions in the reactor. Pressure gauges (McDaniel Controls Inc.), with reading up to 300 psi, were connected to both inlet gas stream tubes and the main reactor to monitor the pressures. Schematics of the membrane holder and the sweep gas flow system are shown respectively in Figure 7 and Figure 8. The sweep gas would flow in from the inner tube of the two concentric tubes and carry away the permeate gas from the back of membrane to outlet through the outer tube with eight holes. The outlet flow was measured using a soap bubble flowmeter. One bypass stream was obtained with a valve to get samples of inlet gases. For the safety purpose one 80 psi gas relief valve was connected to the main reactor. A horizontal split-tube furnace (Mellen™ SV-12, donated by Metcon Inc.) controlled by an Omega™ controller (CN9600), was used to heat the reactor and maintain it at the desired temperature.

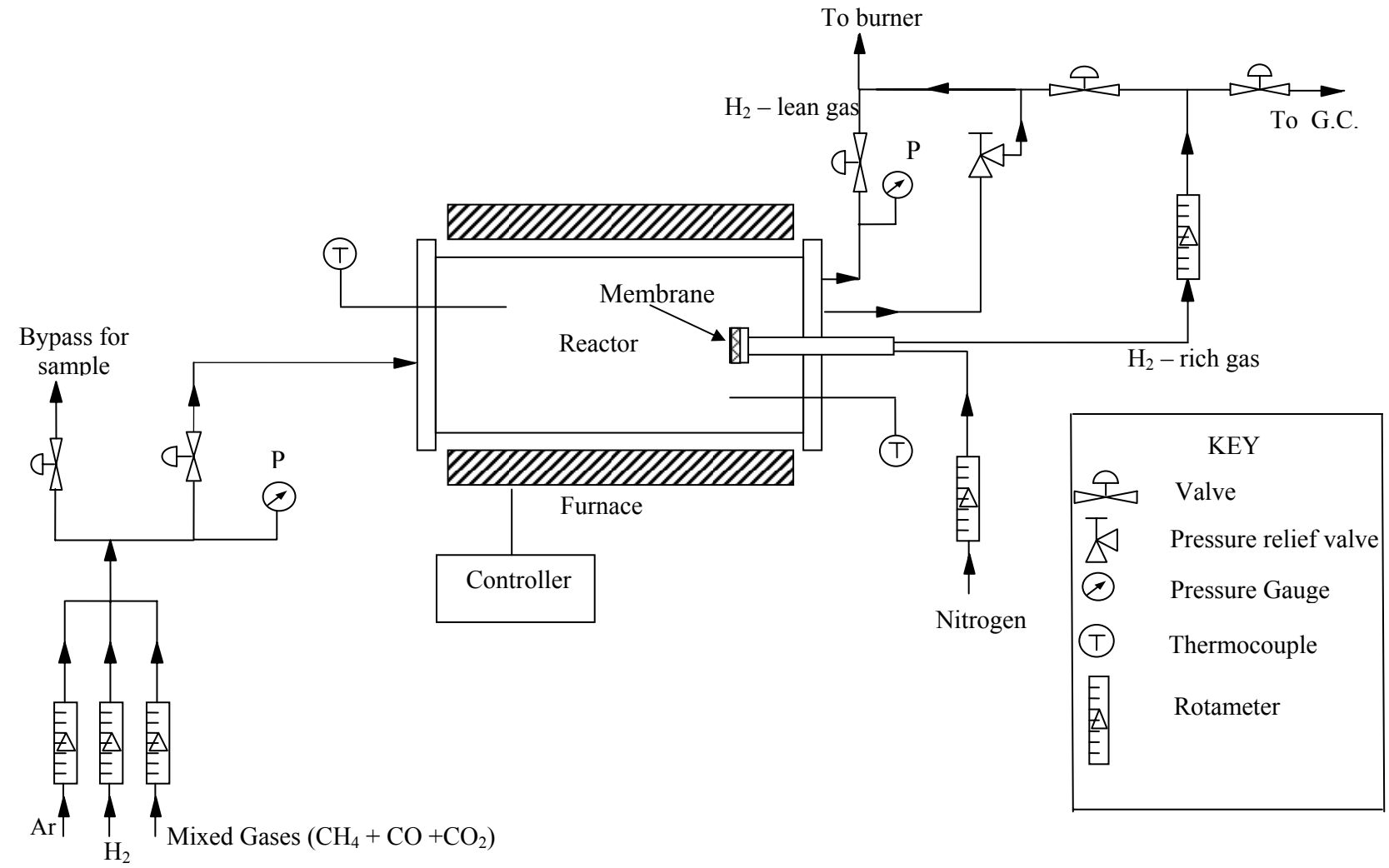

Figure 6 Schematic of experimental setup to measure H_2 permeability

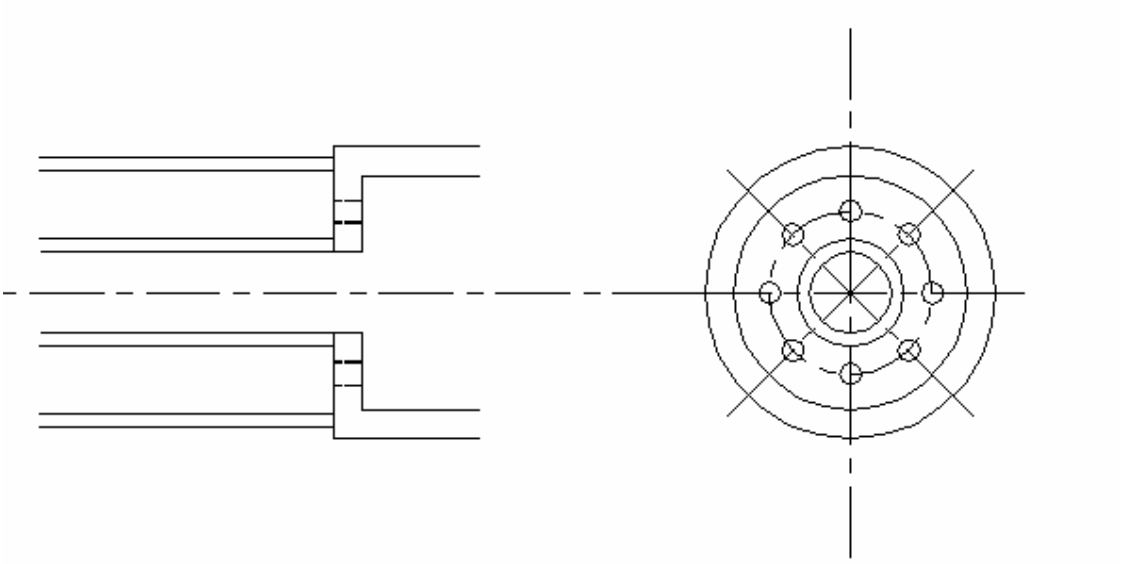

Figure 7 446 Stainless steel holder for holding sample membrane

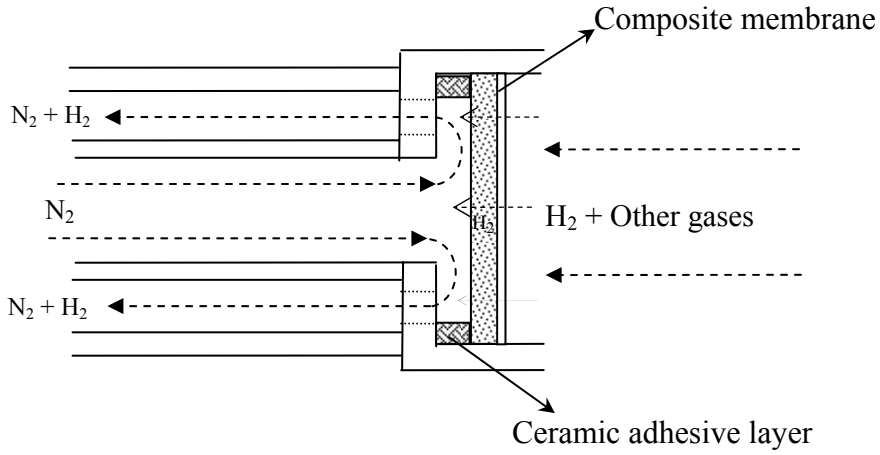

Figure 8 Schematic of gas flow for permeate side

Ceramics and metals have different coefficients of thermal expansion (CTE) and when the membranes are heated, cracks can form in the ceramic part or in the sealant used to seal the ends. To minimize or avoid cracks due to differences in the coefficients of thermal expansion, based on input from Ceramatec Inc., the membrane holder was made from stainless steel 446(ss-446). This steel has a lower CTE than other metals and matches with the CTE of Ceramatec® membranes. Commercially available Resbond 940 (Cotronics Corp.) high temperature ceramic adhesive was used to glue the membrane to metallic membrane holder. Ceramatec Inc. also provided s-glass gel for sealing the membranes to the membrane holder. However, s-glass gel worked fine at room temperature only. At high temperature cracks developed and the seal did not work. It was observed that some carbon black was formed around the area where ceramic adhesive was used. It was believed that as CO and CO_2 were reduced by reducing agent in the ceramic adhesive.

In the experiments, the reactor was first heated to the desired temperature of up to 1300°F and then mix gases ($CO+CO_2+CH_4$), H_2 and/or argon were introduced into the reactor and the desired concentrations were maintained with the flowmeters. The experiments were done at constant pressure and continuous flow of gases into the reactor. The total pressure in the reactor was varied, in different runs, from 40 psi to 80 psi. The pressure in the reactor was maintained by maintaining/controlling the flow rate of exit gases. All the readings were taken after at least 20 minutes at stabilized temperature, pressure and the flow rates of gases. The flow rate of permeate gases swept/carried by N_2 was measured using soap bubble flowmeter. The feed side gases coming out of the reactor were burned

to avoid buildup of inflammable and poisonous gases in the laboratory. The inlet gases and the permeate gas samples were collected in SKC™ sample bags. The sample bags were always vacuumed prior to use to ensure that no residual air was in the bags, which might alter the results from the gas analysis data. The gas samples were analyzed by gas chromatograph (GC) with a thermal conductivity detector (SRI® 8610C) and two separation columns. The GC has a 3-foot Silica-gel, molecular sieve in 0.0125 inches in O.D., in a metal packed column. The gas chromatograph analyzed the gases to help determine the mole fractions of nitrogen, methane, carbon monoxide, carbon dioxide and hydrogen. A Gateway® 2000 computer with Peaksimple 1.44 software controlled the gas chromatograph operation and analyzed the gases.

Data Reproducibility

To determine the accuracy of the experimental procedures, some of the experiments using both the membranes, Ceramatec® membrane and Pd/Al_2O_3, were repeated. The test of reproducibility of data was done in two ways. First, the experimental conditions were kept the same as one of the previous runs and data were obtained to check whether similar results were obtained or not. Second, the experiments were done at conditions close to an earlier done experimental run and then the result was checked to see how it fell with respect to a curve fit through previously obtained data. The test of reproducibility of data was done atleast once at each temperature. The error analysis showed an average error band of 10%. The maximum error was found to be around 15% and the minimum value was around 3%-4%.

5. DATA ANALYSIS

Raw Data Analysis

Data from the reactor operation with the membranes and the gas chromatograph analysis data obtained during each experimental run were used to determine the permeate gases and H_2 permeation fluxes. The mole fractions of the feed gases and the permeate gases were calculated from their corresponding response peak areas from the GC output and peak areas from standard calibration gas mixture. For calibration three different gases obtained from BOC were used. One calibration gas had a molar composition of 10% methane, 35% carbon monoxide and rest carbon dioxide. Other calibration gases used were pure nitrogen and pure hydrogen. The mole fractions of gases in samples were determined using argon as carrier gas. From the gas chromatograph results, the mole fraction of the individual gas component, y_i with peak area A_i, at each time interval were calculated using:

$$y_i = \left(\frac{y_{cal,i}}{A_{cal,i}} \right) A_i \qquad (5.1)$$

The mole fractions of the calibration standards and the corresponding calibration peaks areas are symbolized by $y_{cal,i}$ and $A_{cal,\ i}$ .A small amount of air apparently was inadvertently entrained into the gas chromatograph during sample injection. This inadvertent contribution of oxygen and nitrogen from leaked air was corrected and the mole fractions of the gases of interest were normalized.

Flow rates were measured using a soap bubble flowmeter and times for traveling the volume of 20 cc (V_L). Readings from bubble flowmeter were taken before and after samples were collected.

$$t_{avg} = \frac{t_1 + t_2}{2} \quad \text{(s)} \qquad (5.2)$$

$$v = \frac{V_L}{t_{avg}} \quad \text{(cc /s)} \qquad (5.3)$$

$$J_{H_2} = v \times y_{H_2,Perm} \quad \text{(cc of } H_2 \text{ /s)} \qquad (5.4)$$

Where t_1 and t_2 are the times associated with readings of the flowmeter for a flow of V_L= 20 cc of permeate gas sample, before and after the samples were collected. Fluxes of hydrogen across the membrane were calculated using the mole fraction of hydrogen and the volumetric flow rate. The partial pressure of hydrogen on the feed side was obtained from,

$$P_{H_2} = y_{H_2,Feed} \times P_{reactor} \qquad (5.5)$$

In the hydrogen permeation experiments, when the membrane was not gas tight, the real fluxes of hydrogen had to be calculated by using a subtraction method. For these cases of leakages, if the total hydrogen diffusion through the membrane and hydrogen diffusion through only the pinholes are known, then the net hydrogen diffusion through the dense metal part can be calculated as:

$$J_{H_2(metal)} = J_{H_2(Total)} - J_{H_2(pinhole)} \qquad (5.6)$$

Palladium is permeable only to hydrogen. So on the permeate side, if apart from hydrogen, other gases were also present, then these gases present on the permeate side of the membrane must have crossed through the pinholes in the membrane. The ratio mole fraction of hydrogen to methane, on the feed side was used to calculate the corrected mole fraction of hydrogen. The corrected mole fractions of hydrogen on the permeate side of the membrane were given by:

$$y_{H_2,metal} = y_{H_2,Total} - y_{CH_4,Total} \times \frac{y_{H_2,Feed}}{y_{CH_4,Feed}} \qquad (5.7)$$

Since GC provides the analytical results in terms of volume or mole fractions, it was advantageous to use this correction in terms of mole fractions rather than in terms of mass fractions and mass flow rates.

Ceramatec® Membrane

The membrane provided by Ceramatec Inc. was a ceramic-ceramic composite material in which independent migration of proton and electron species occurs through an interpenetrating network of proton and electron conducting ceramic phases (46). The ceramic-ceramic composite material developed is proprietary and the composition has not been disclosed. This dense ceramic membrane was also tested for permeability of hydrogen under a simulated syngas environment. Experiments were carried out at different pressures and temperatures. The temperature was varied from 70°F (i.e. room temperature) to 1300°F (typical exit temperature in a catalytic gasifier). Total pressure

was varied from 30 psi to 80 psi. Flux and permeance measurements obtained at different temperatures were plotted against the partial pressure of hydrogen on the feed side. The plots of flux of hydrogen against partial pressure of hydrogen, at different temperatures, are given in Figure 9-14. In Figure 15 hydrogen flux was plotted against partial pressure raised to power 0.61. It is clearly seen in these figures that the hydrogen permeation fluxes are partial pressure/concentration driven. It was seen that both linear and power fitted to experimental data very well. So, just from data and without knowledge of exact composition, it is difficult to say the exact relationship between hydrogen flux and feed side hydrogen partial pressure. The maximum hydrogen flux by diffusion was found to be 0.0321(mol/m^2 s), calculated at normal temperature and pressure (NTP) of 293.15 K and

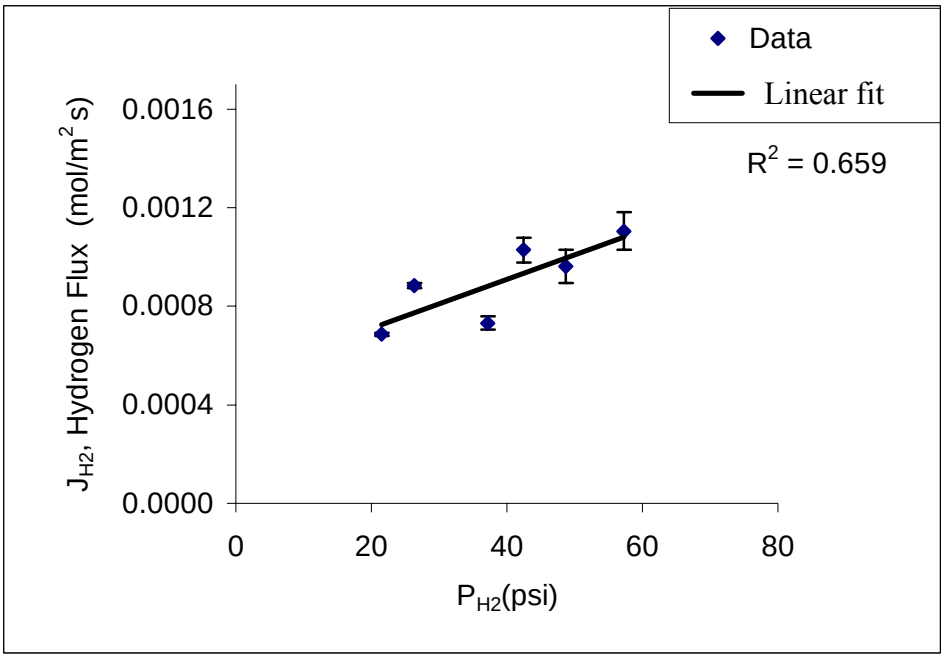

Figure 9 J_{H2} vs. P_{H2} at 70°F for Ceramatec® membrane

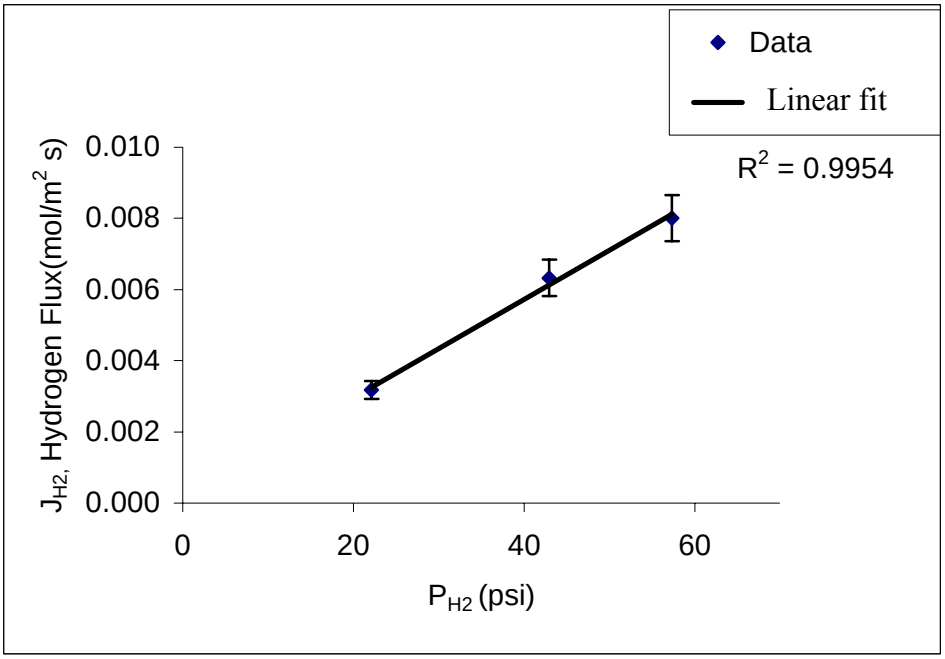

Figure 10 J_{H2} vs. P_{H2} at 500°F for Ceramatec® membrane

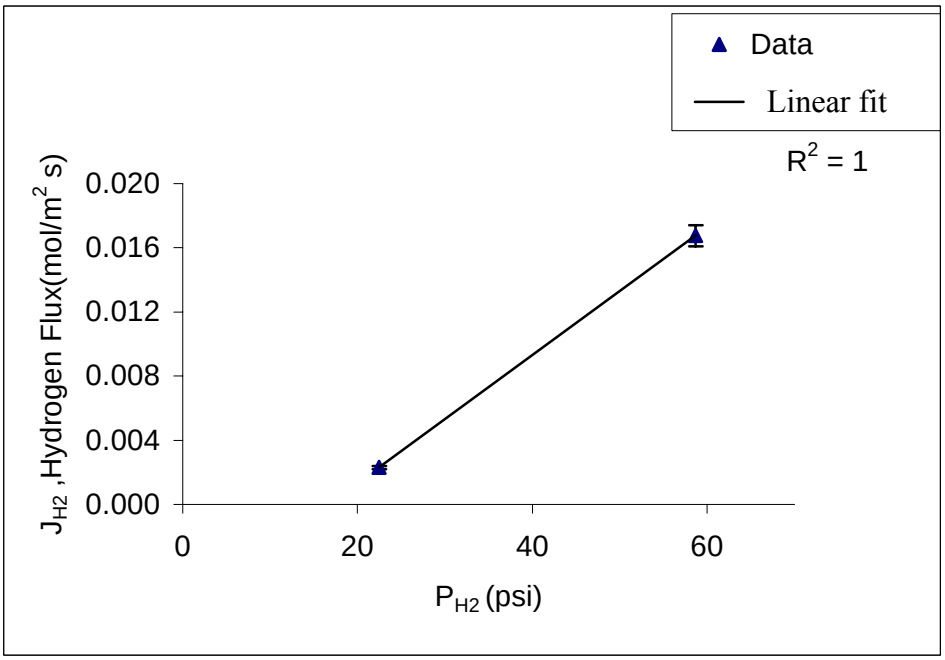

Figure 11 J_{H2} vs. P_{H2} at 700°F for Ceramatec® membrane.

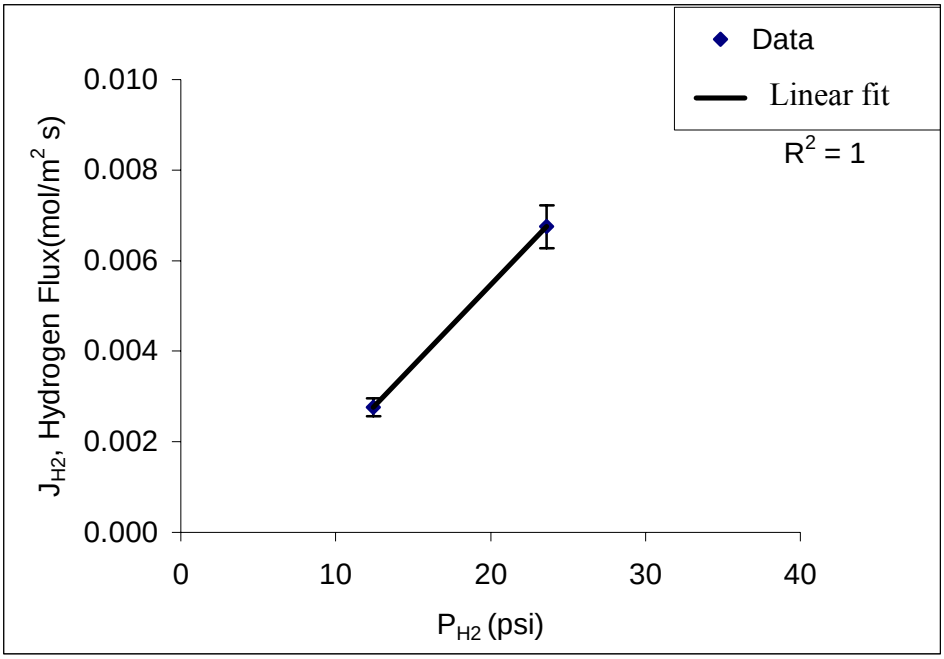

Figure 12 J_{H2} vs. P_{H2} at 900°F for Ceramatec® membrane.

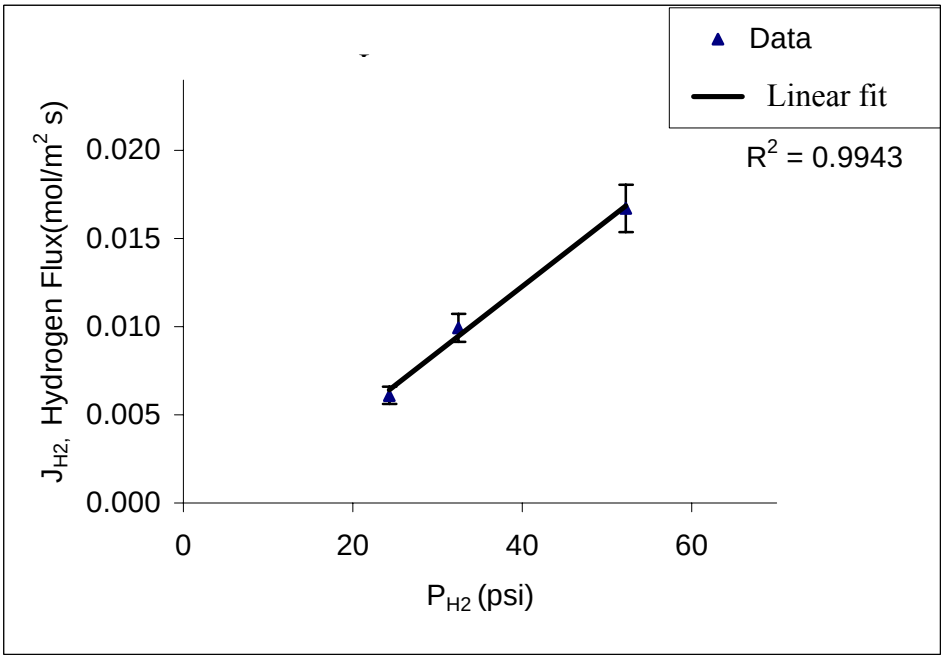

Figure 13 J_{H2} vs. P_{H2} at 1100°F for Ceramatec® membrane.

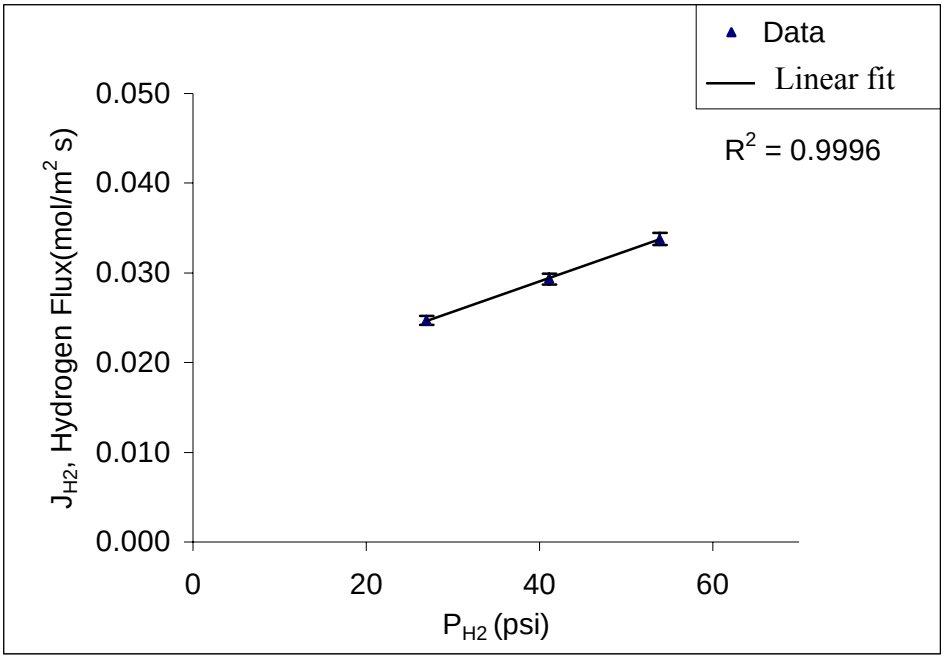

Figure 14 J_{H2} vs. P_{H2} at 1300°F for Ceramatec® membrane.

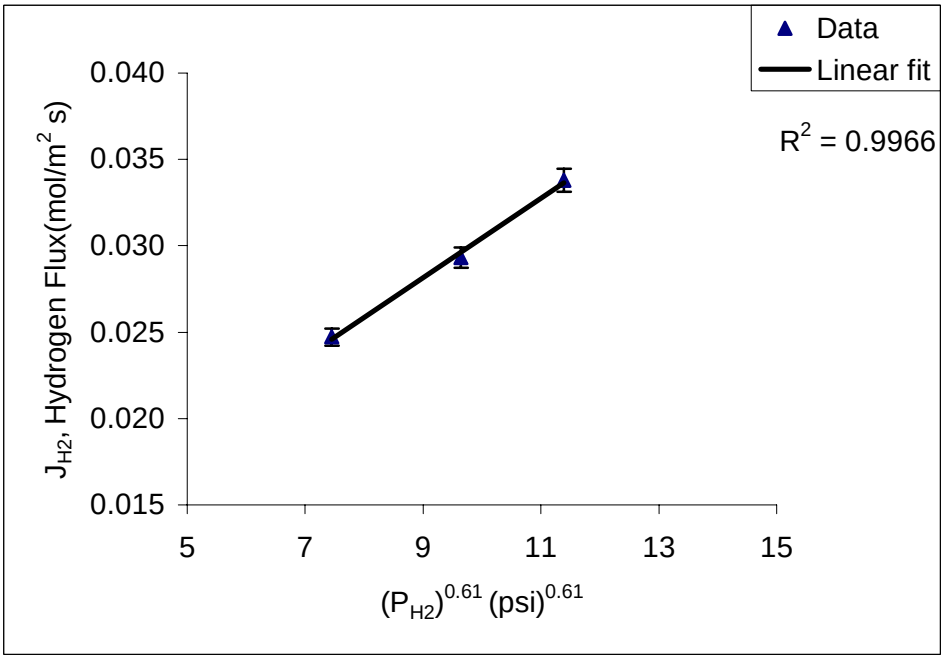

Figure 15 J_{H2} vs. $(P_{H20})^{0.61}$ at 1100°F for Ceramatec® membrane

1 atmosphere, respectively. These values were well within the range reported by Ceramatec Inc. Ceramatec Inc. has published the hydrogen permeation flux of 0.1362 ± 0.272 (mol/m^2 s) for their 35 μm thick membranes and 0.0095 ± 0.0020 (mol/m^2 s) using their 500μm thick membranes. Ceramatec Inc. conducted these experiments at 900°C in which the feed side gases were at 1 atmosphere and the product side was continuously swept with nitrogen. Also the feed side mole fraction of H_2 was varied from 0.3 to 0.6.

The thicknesses of the membranes provided by Ceramatec Inc. for the present study were not known. Assuming that the thicknesses of the membranes in this study was within the range of 35-500μm, the results obtained in this work were in good agreement with the results of Ceramatec Inc. Also, the present experiments were conducted at a slightly lower temperature of 1300°F, compared to the maximum temperature of 1650°F in experiments by Ceramatec Inc.

Table 4 provides the hydrogen permeation fluxes of Ceramatec® membranes and a few other proton-conducting ceramic membranes reported in the literature. Since only limited hydrogen permeation data through proton-conducting ceramic membranes are available in the open literature and those experiments were conducted under different conditions, it is difficult to compare permeation flux under identical conditions. Table 4 also shows that the hydrogen permeation flux of Ceramatec® membrane is comparable with well studied proton-conducting ceramic membranes by other researchers.

Table 4 Summary of results for H_2 separation using ceramic-membrane

Membrane	Thickness (μm)	Temperature (K)	H_2 Flux (mol/m^2 s)	ΔP_{H2} (kPa)	Reference
Ceramatec® Membrane	500	1173	0.0095	60.8	46
Ceramatec® Membrane tested at UTSI	unknown	295-978	0.0008-0.0321	172-379.2	This work
Ceramatec® Membrane	35	1173	0.1362	60.8	46
$SrCe_{0.95}Tm_{0.05}O_{3-\delta}$ (SCTm)	1600	1173	0.00029	20.3	49
BCY-Pd	230	1173	0.0082	101*	50
$SrCe_{0.95}Y_{0.05}O_{3-\delta}$ (SCYb)	1100	1073	0.0005	unknown	51

* pressure gradient of H_2 across the membrane was 100% / 0.01%

Dorris et al. (51) provided data on the gradient of H_2 across the membrane in the terms of relative molar ratio of hydrogen to the other constituents. These values were 4% on the feed side and 0.488% on the permeate side. However, there was not enough information provided to calculate ΔP_{H2} value.

For the Ceramatec® membrane it can be observed that the hydrogen permeation flux is inversely proportional to thickness of the membrane. Or, it can be calculated that product of thickness and hydrogen permeation flux is constant. The value of the constant calculated from the data published by Ceramatec Inc. was 4.76×10^{-6} (mol/m.s). Figure 16 shows the curve relating thickness of membrane and hydrogen permeation flux. The permeation flux data for Ceramatec® membrane at 1300°F, obtained in this work, has been also shown. The thickness calculated from this curve was 144 μm. This calculation is not accurate and it is just approximate calculation of the thickness. This curve also support that the hydrogen permeation flux data from the current work is within the range of values published by Ceramatec, Inc.

Characterization of Palladium and Platinum Membranes

X-Ray diffraction (XRD) analysis of the Pd membranes fabricated in the present study were carried with 2θ changed from 20 to 100° using a Philips Norelco diffractometer with CuKα radiation (1.56Å) at 20 kV and 2 mA setting and 0.02°/min scan speed. Study of the surface morphologies of the membranes were carried out using SEM and optical microscope. Thicknesses of the metallic films were also determined using SEM and

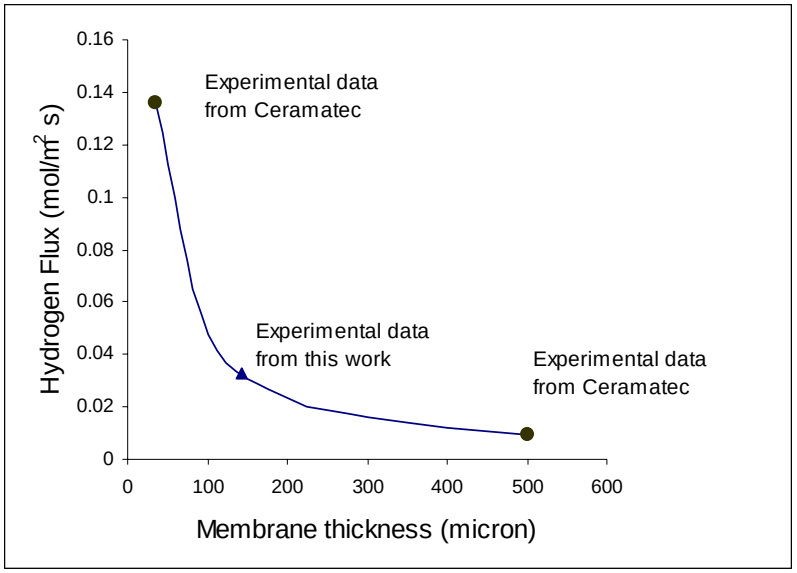

Figure 16 Curve relating J_{H2} and Ceramatec® membrane thickness

optical microscope. Figure 17 is X-Ray diffraction (XRD) spectrum of the α-alumina substrate. Apart from the major peaks of α-alumina, SiO_2 peaks were also present due to the impurity present in α-alumina substrate. Figure 18 is XRD spectrum of γ-alumina layer on α-alumina substrate. Peaks corresponding to γ-alumina were not present. There absence could be due to transition of this metastable high temperature phase into stable low temperature phase α-alumina. XRD spectrum of the top layer of Pd on Al_2O_3 (Figure 19) revealed face-centered cubic Pd. These peaks of palladium confirm the formation of pure palladium, on the γ-alumina coated α-alumina substrate. Peaks of α-alumina and SiO_2 were also identified, as marked in the XRD spectrum. This is because the X-rays penetrate the samples to the depth greater than the thickness of the Pd metal film. Figure 20 is the XRD spectrum of top layer of Pt on Al_2O_3. SiO_2 and α-alumina peaks were also identified in XRD spectrum of Pt on Al_2O_3.

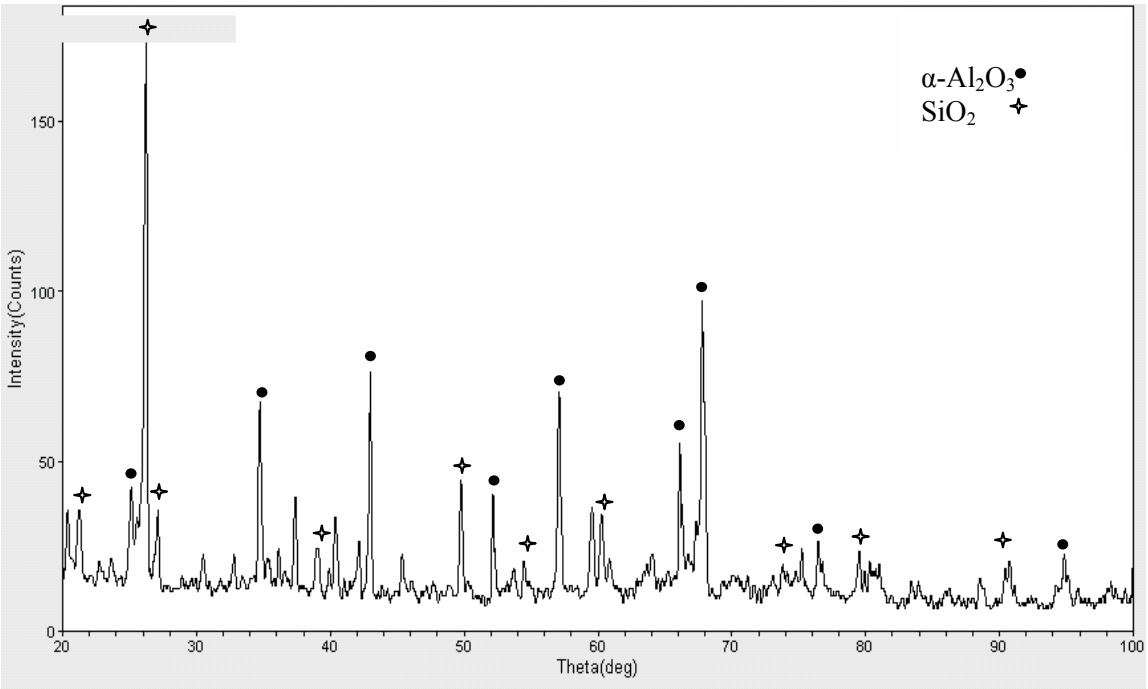

Figure 17 X-Ray diffraction spectrum of α-alumina substrate.

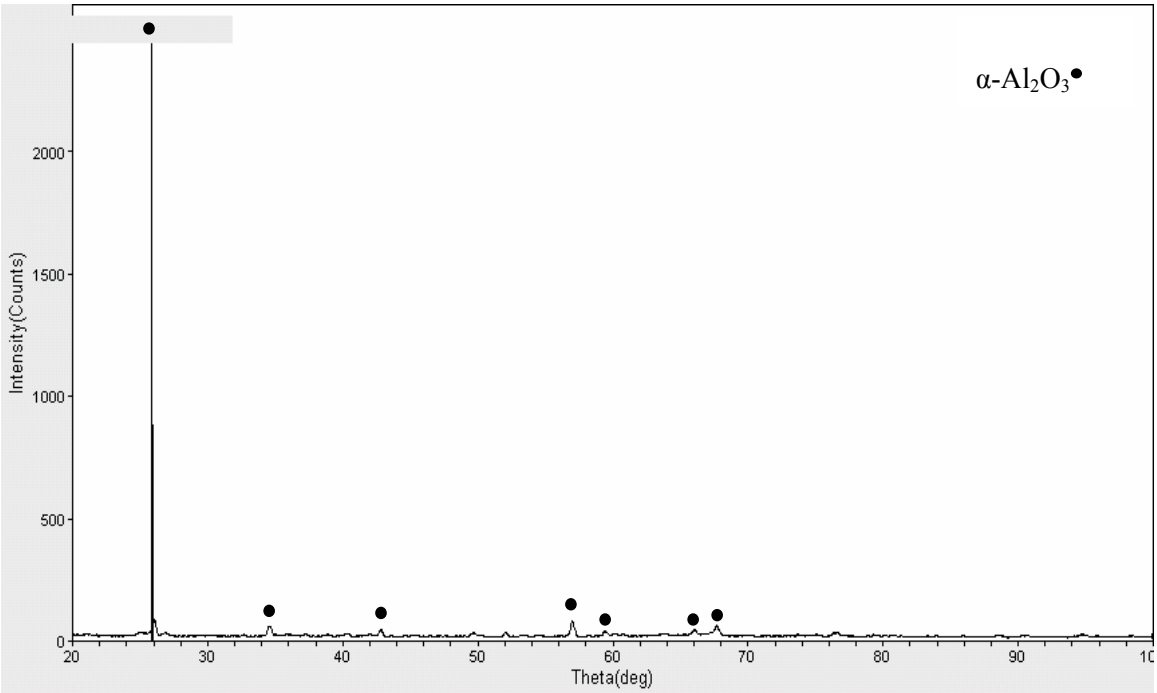

Figure 18 X-Ray diffraction spectrum of γ-alumina layer on α-alumina substrate.

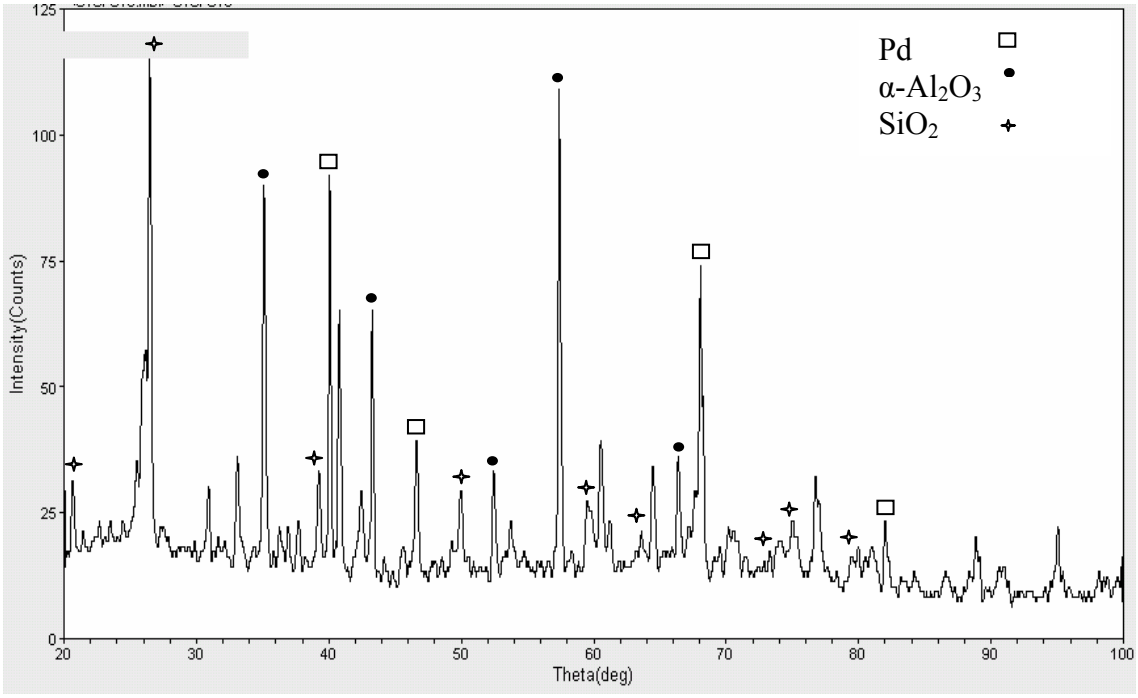

Figure 19 X-Ray diffraction spectrum Pd/Al_2O_3 membrane.

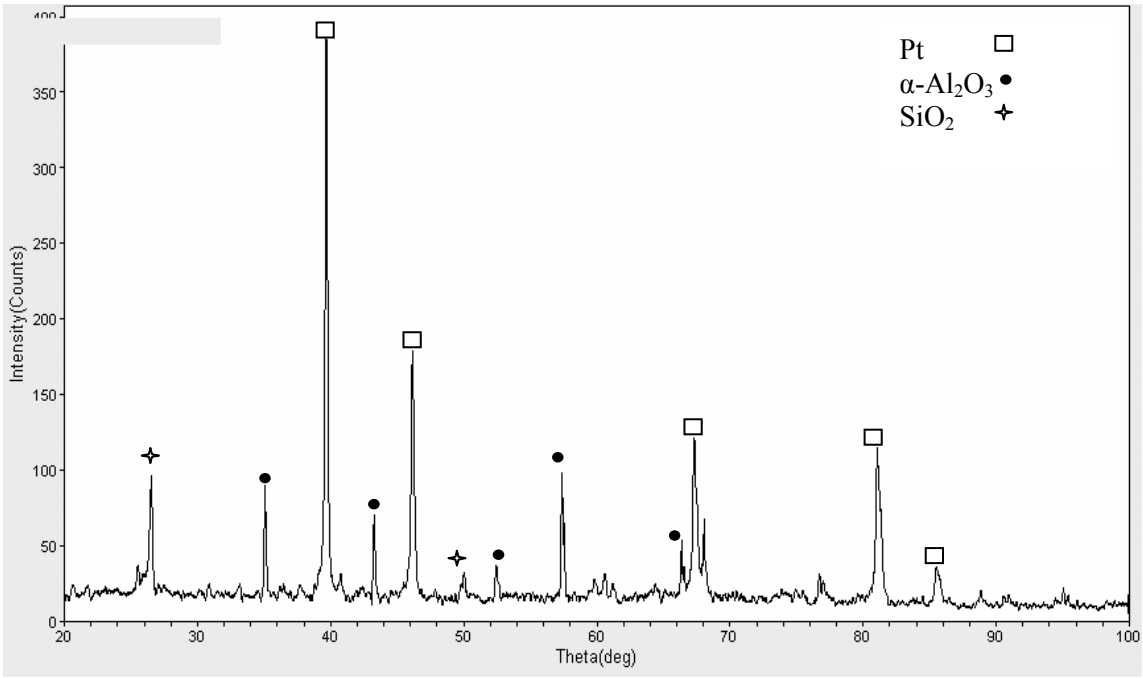

Figure 20 X-Ray diffraction spectrum of Pt/Al_2O_3 membrane.

The surface morphologies of the α-alumina substrate and the modified surface after being coated with γ-alumina, are shown respectively in Figure 21 and Figure 22. It can be seen that the grain structure of the α-alumina surface has more voids and appears rougher than the surface morphology after coating with γ-alumina (Figure 22). The surface of γ-alumina layer is shinier than that of α-alumina implying a smoother surface.

Figure 23 and Figure 24 show the low magnification optical images of the surfaces of the Pd-membrane and Pt-membrane supported on the above-mentioned composite ceramic substrate, respectively. The surface morphology of the coating appears uniform and smooth. The coated films showed good adhesion on the support.

Figure 25 and Figure 26 are cross-sections showing the Pd and Pt layers on ceramic substrates. The palladium layer has formed on the surface of the alumina substrate. In the case of platinum it was observed that platinum layer was formed on the top of alumina substrate and also some platinum infiltrated deep inside the pores. This happened because the platinum precursor was totally soluble in water and when the layer was applied to alumina substrate, it probably seeped inside the pores. This kind of deposition did not happen with the palladium layer since the palladium precursor formed slurry and the particles did not go deep inside the pores. Thickness of Pd layer was estimated to be 77 μm and for the Pt layer it was about 72μm.

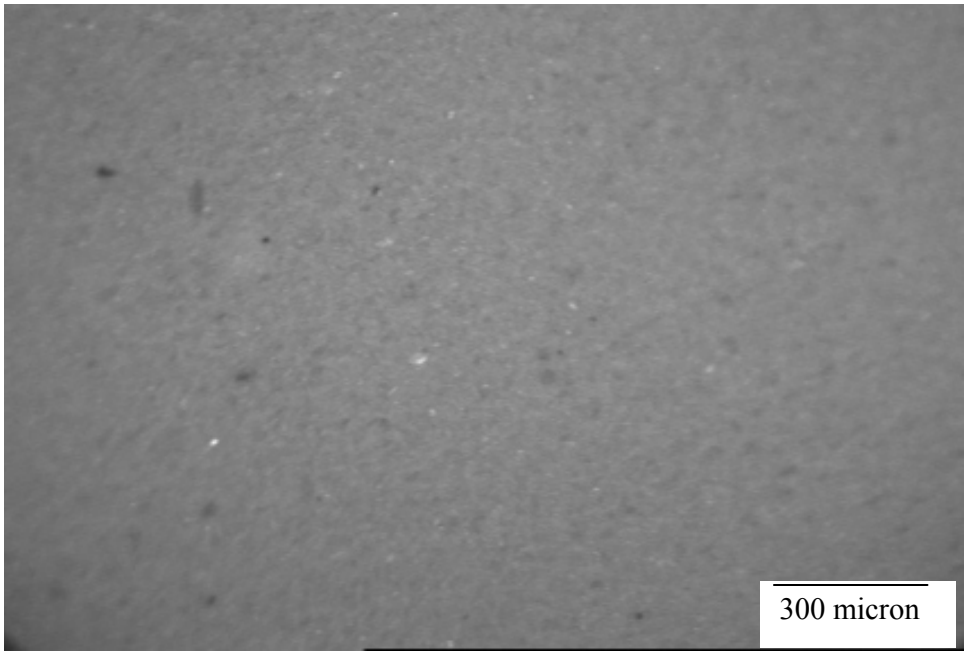

Figure 21 Surface morphology of α-alumina substrate.

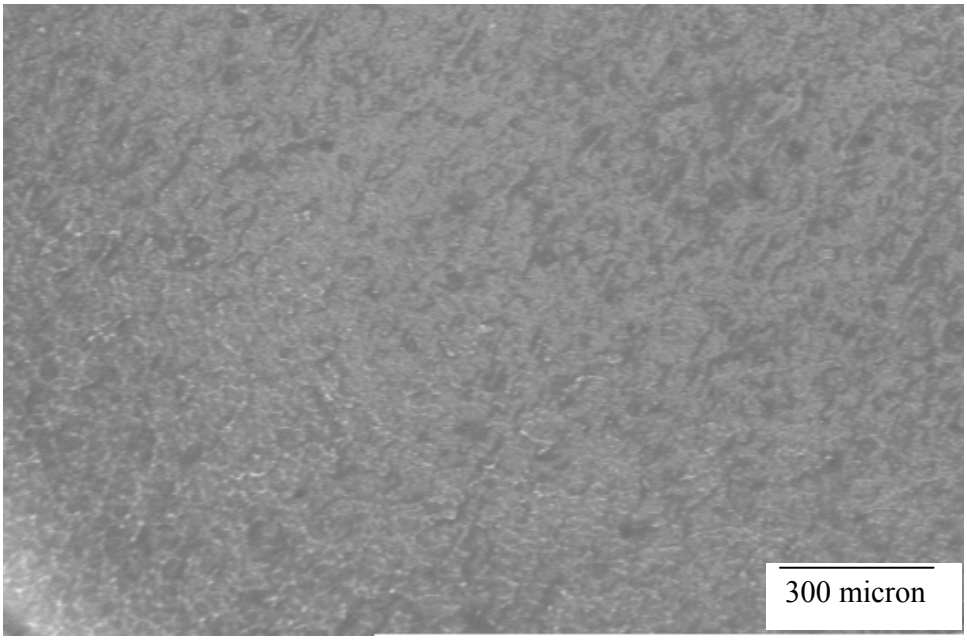

Figure 22 Surface morphology of γ-alumina layer.

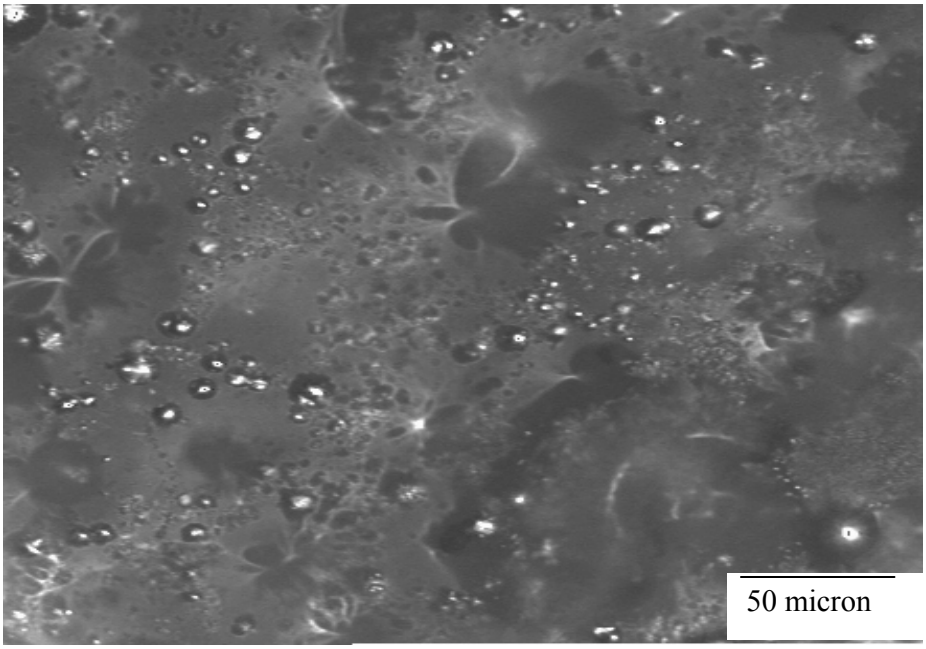

Figure 23 Surface morphology of the Pd-membrane.

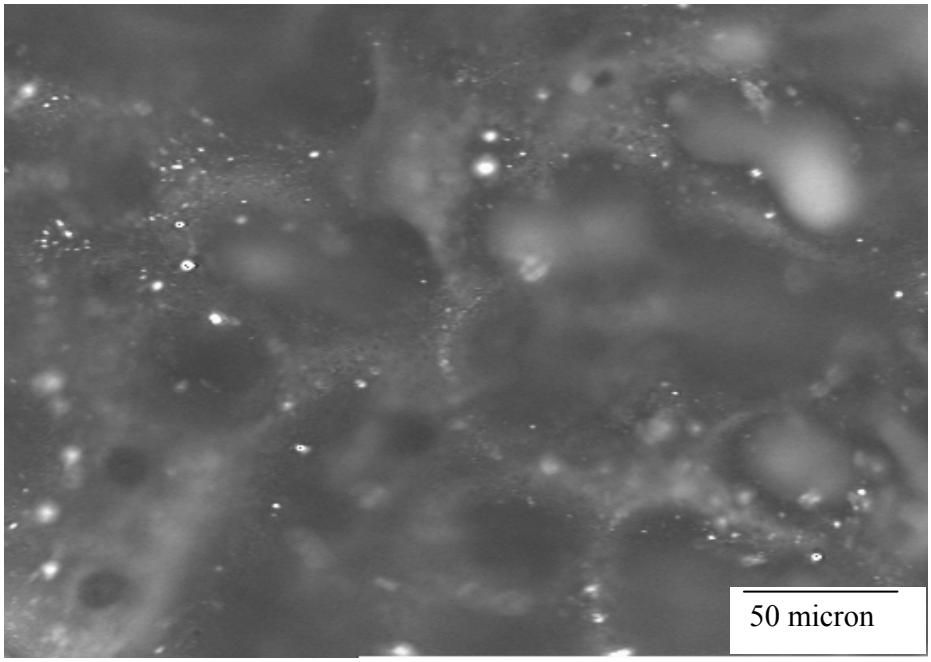

Figure 24 Surface morphology of the Pt-membrane.

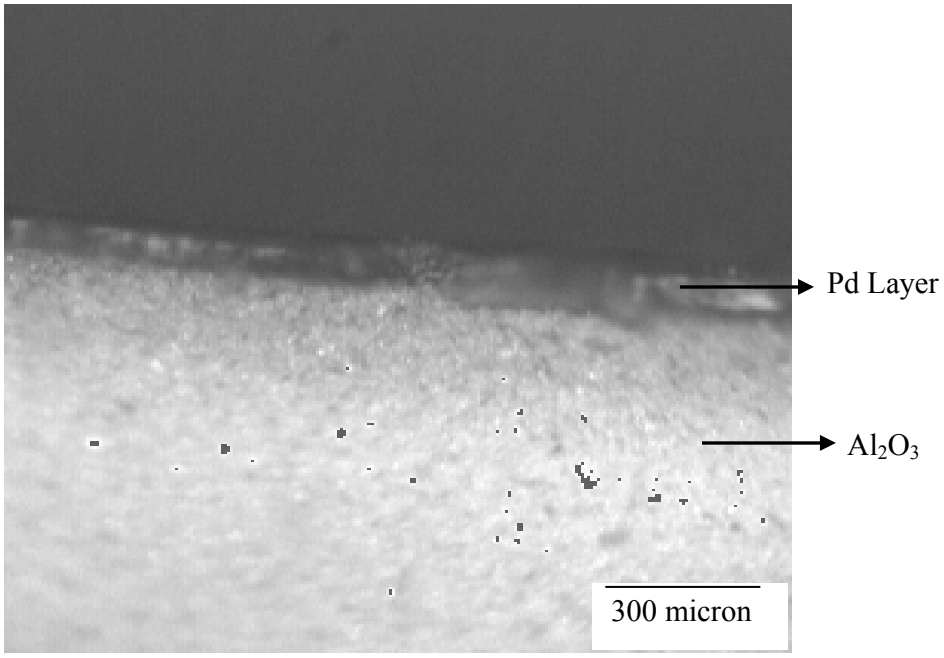

Figure 25 Cross-section of Pd-layer on Al_2O_3

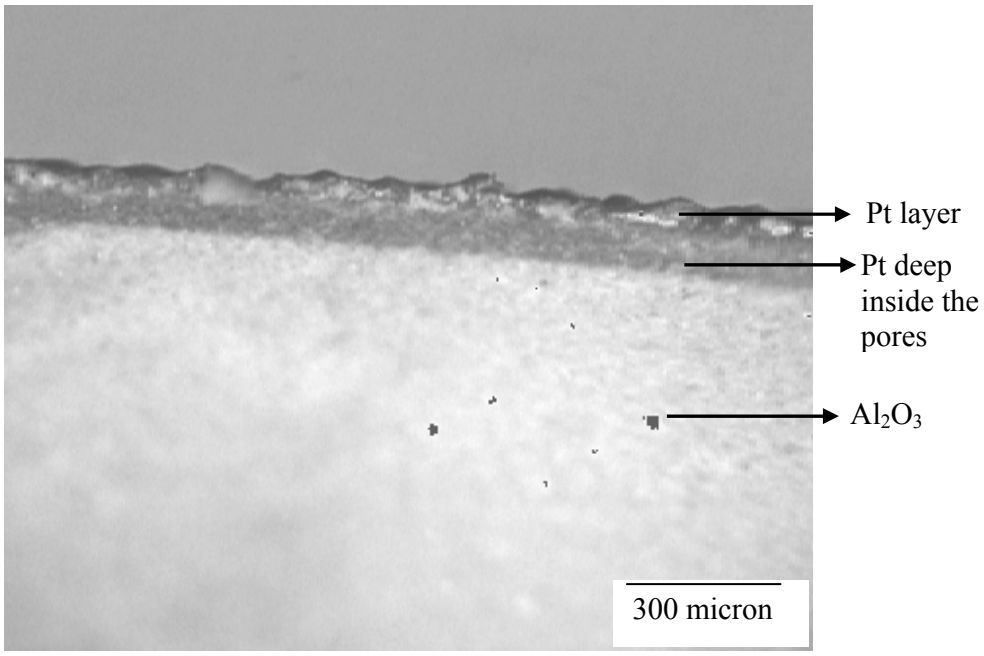

Figure 26 Cross-section of Pt layer on Al_2O_3

In Figure 27, the shining patches across the membrane are the areas corresponding to overlapping of the laser beam during processing. We can see that this area of overlap looks smoother than the other parts. This surface was laser treated twice because the laser beam was traced in straight, overlapping stripes so that entire surface of the sample was covered. It was observed that the metallic layers in overlapping areas were smooth and even. This observation indicates that in the future, pinholes in the metallic film can be plugged by laser treating the already formed metallic layer.

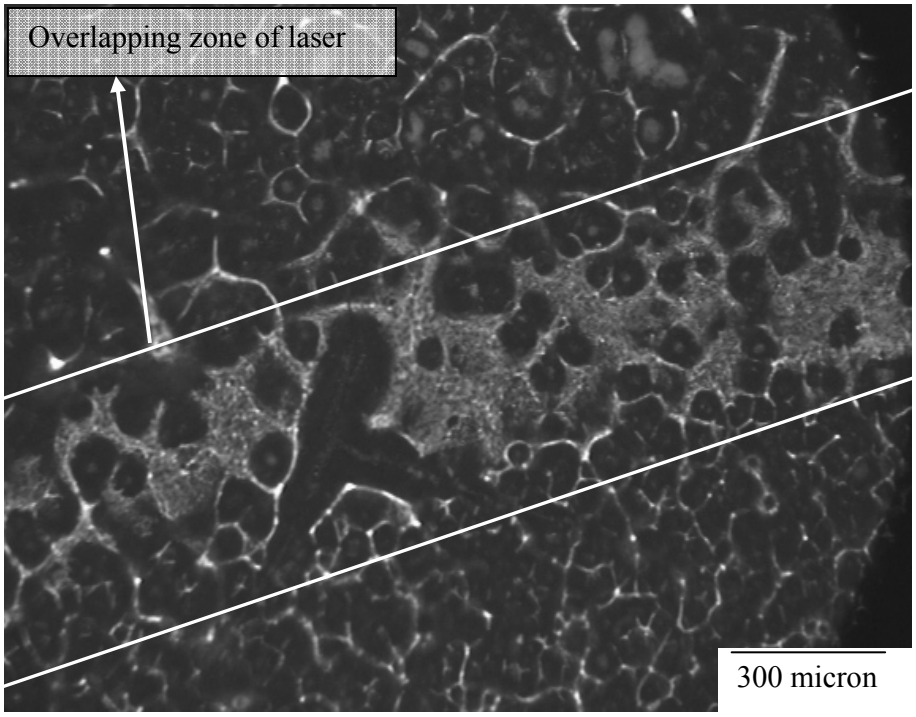

Figure 27 Palladium surface showing overlapping area of laser treatment.

Hydrogen Permeation Results for Palladium Membrane

Figure 28-30 show the variation of hydrogen flux with hydrogen partial pressure for palladium membrane at different temperatures. As discussed in Chapter 3, hydrogen flux through a membrane was represented by Eq. 3.1 as a function of hydrogen partial pressure, the permeability constant of the membrane material, and the thickness of the membrane, X_M. Also, the driving force for hydrogen permeation through the membrane is directly proportional to the difference in the hydrogen partial pressures of the retentate and permeates, each to the power 'n'. The partial pressure exponent 'n' was calculated by fitting a power curve through the hydrogen flux and the difference in the hydrogen partial pressures. In this experiment, since all hydrogen was continuously swept off from permeated side of the membrane by nitrogen used as the sweep gas, so the partial pressure term on permeate side became essentially zero and thus the driving force was equal to the hydrogen partial pressure on the feed side. From the plots (Figure 28-30) pressure exponent 'n' was estimated to be 0.5978, 0.6024 and 0.6188 at 900 ºF, 1100 ºF and 1300 ºF, respectively. The average value of coefficient of regression (R^2) for the fitted curves was 0.9460. A summary of data obtained from the plot is given in Table 5. The average value of 0.61 was used as pressure exponent in further calculations. This average value of 'n' was then used to plot the hydrogen flux data against $P_{H2}^{0.61}$ at different temperatures. Straight lines were fitted to the data and the slope of the line gave the hydrogen permeance (X_M/k) at different temperatures. Using the thicknesses of the membranes, permeability constants at different temperature were calculated. The value of pressure exponent obtained is in the range of values reported in literature. Li et al. (28)

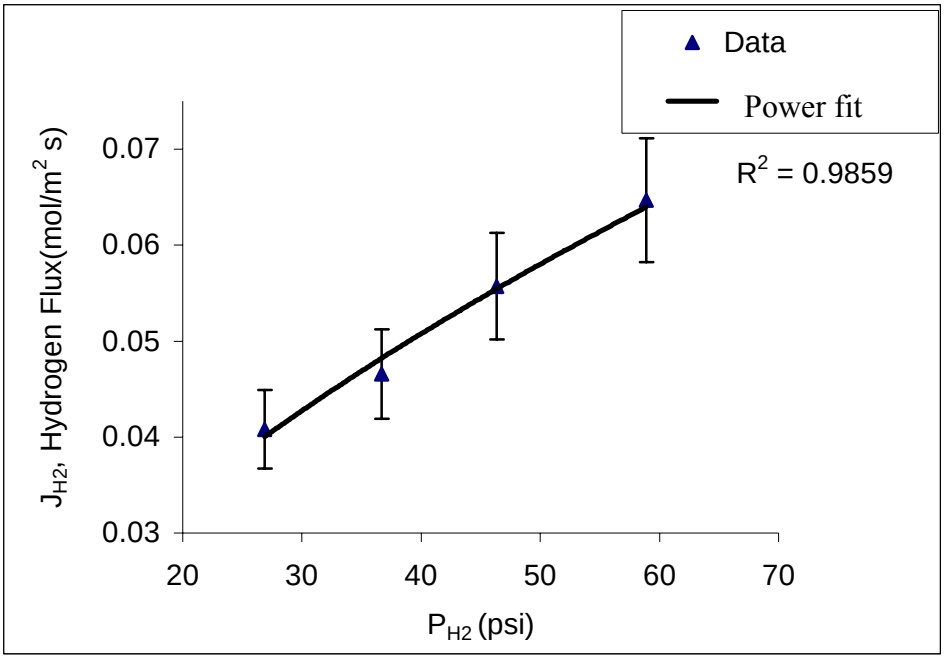

Figure 28 J_{H2} vs. ΔP_{H2} at 900°F for Pd/Al_2O_3 membrane

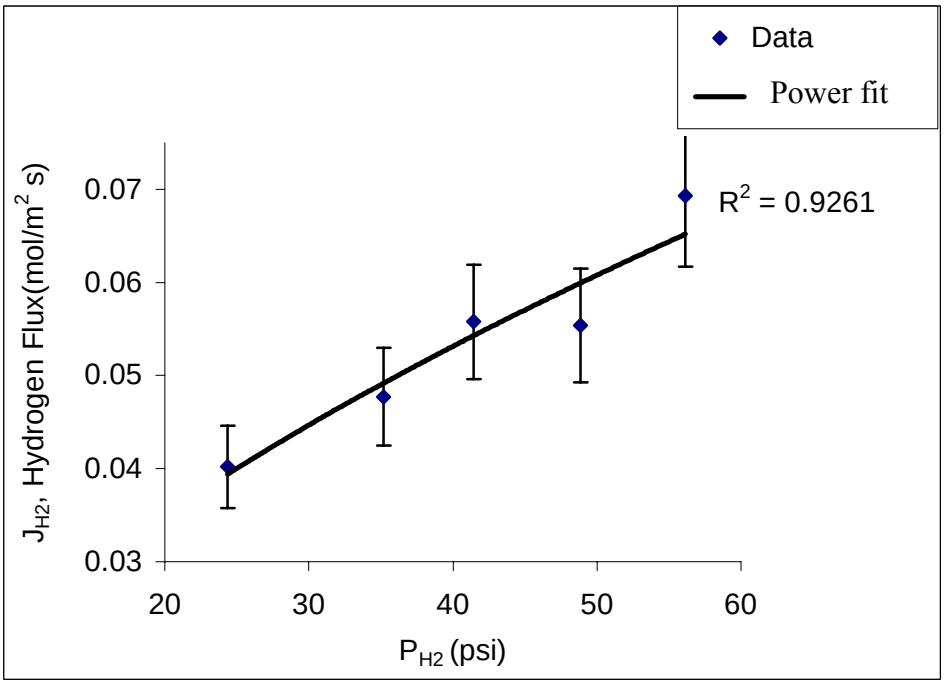

Figure 29 J_{H2} vs. ΔP_{H2} at 1100°F for Pd/Al_2O_3 membrane

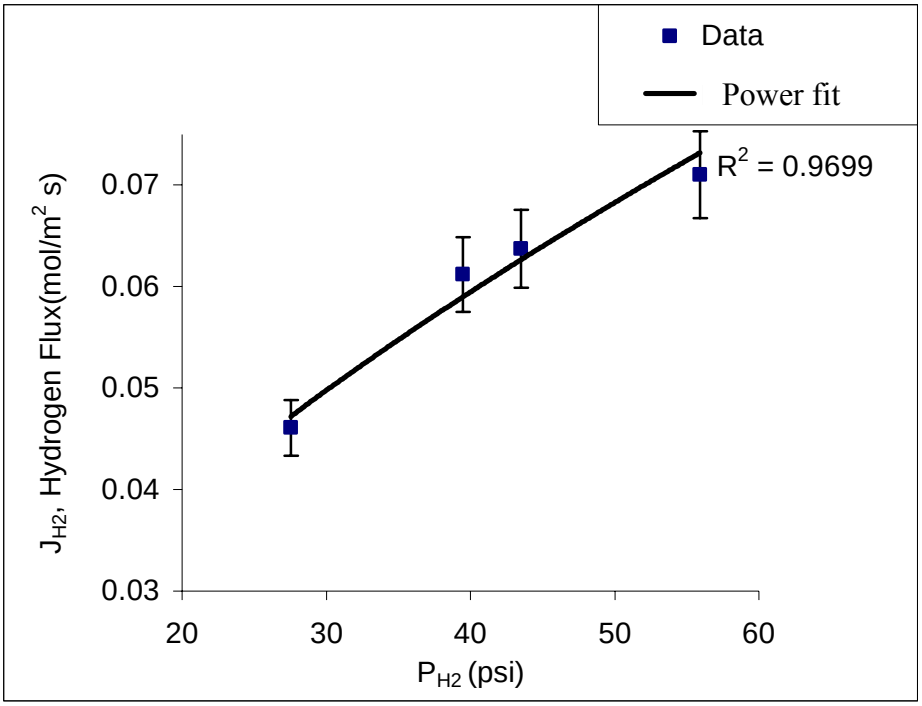

Figure 30 J_{H2} vs. ΔP_{H2} at 1300°F for Pd/Al_2O_3 membrane

Table 5 Summary of results obtained from of J_{H2} vs. P_{H2} plots

Temperature (°F)	Pressure Exponent (n)	Coefficient of Regression (R^2)
900	0.5978	0.9859
1100	0.6024	0.9261
1300	0.6188	0.9699

reported a value of 0.65 for 10μm Pd/Al_2O_3 membranes prepared by electroless plating with osmosis. Collins and Way (52) also reported a value of 0.57 for 17μm thick membrane. Figure 31-33 represent the plots of hydrogen permeation flux against $P_{H2}^{0.61}$ at 900°F, 1100°F and 1300°F respectively. From these plots, the values of permeability constants 'k' were estimated to be 1.876×10^{-09} (mol/m s $Pa^{0.61}$), 2.037×10^{-09} (mol/m s $Pa^{0.61}$) and 2.275×10^{-09} (mol/m s $Pa^{0.61}$) at 900ºF, 1100ºF and 1300ºF respectively. These values of permeability constant 'k' are in agreement with the Collins' and Way's (52) value of 6.82×10^{-09} (mol/m s $Pa^{0.57}$) at 823K. Morreale et al. (53) reported value of 3.21×10^{-08} (mol/m s $Pa^{0.62}$) in the 623-1173 K temperature range for 1mm thick palladium membranes. These results are summarized in Table 6.

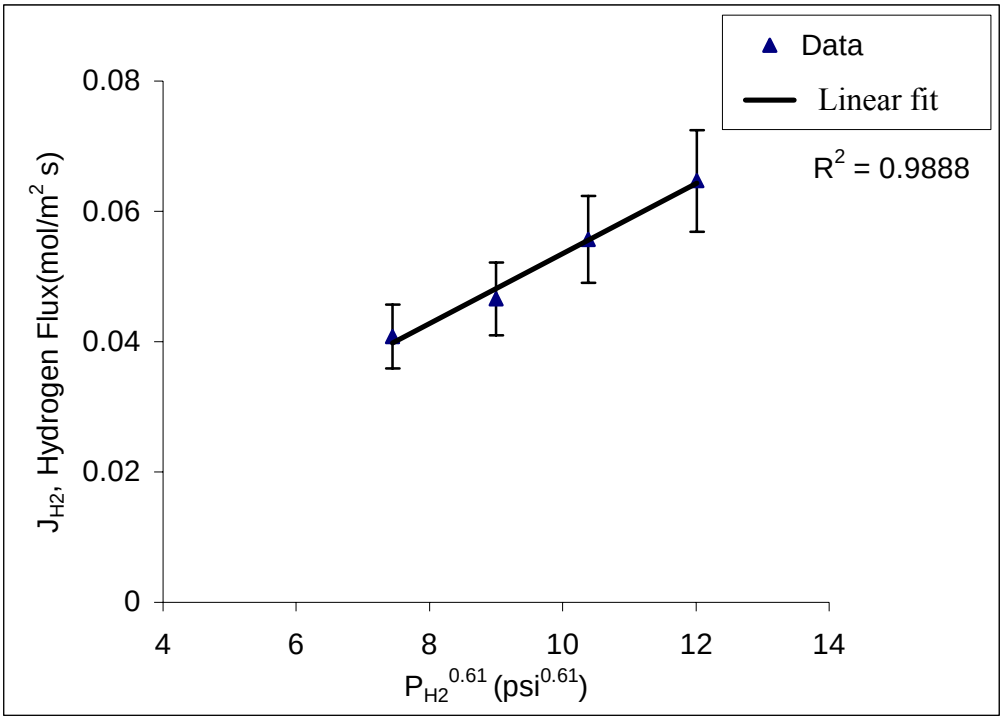

Figure 31 J_{H2} vs. $(P_{H20})^{0.61}$ at 900°F for Pd/Al_2O_3 membrane

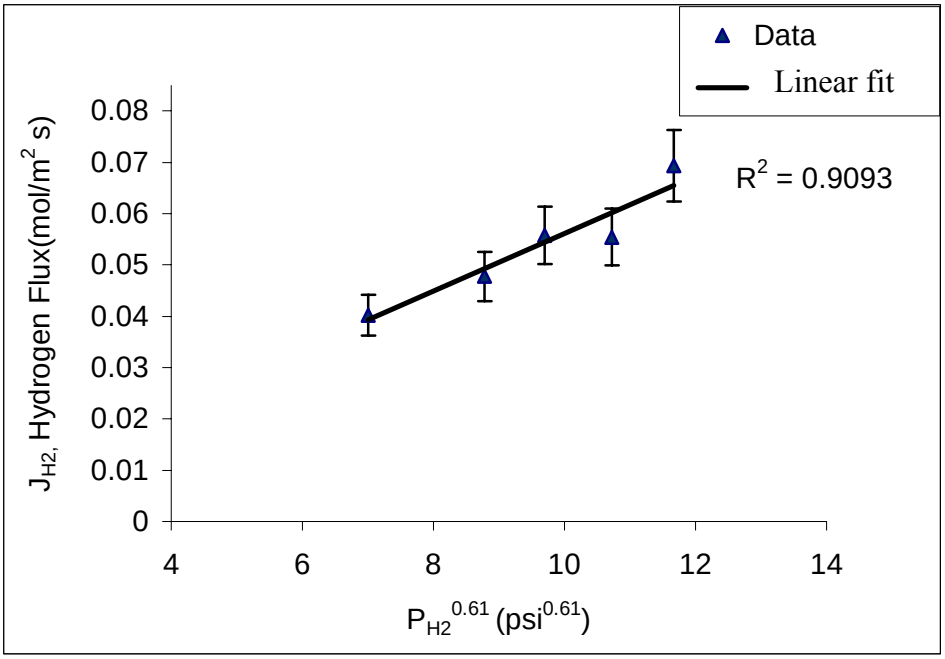

Figure 32 J_{H2} vs. $(P_{H20})^{0.61}$ at 1100°F for Pd/Al_2O_3 membrane

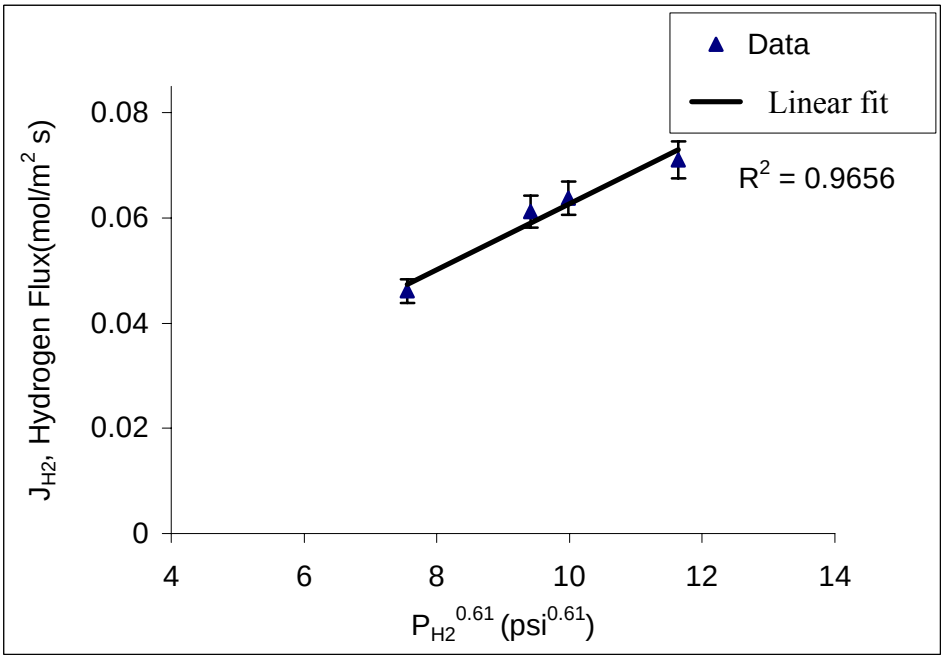

Figure 33 J_{H2} vs. $(P_{H20})^{0.61}$ at 1300°F for Pd/Al_2O_3 membrane

Table 6 Summary of results for Pd/Al_2O_3 membrane

Temperature (°F)	Permeance (k/X_M) ($mol/m^2\ s\ Pa^{0.61}$)	Permeability constant (k) ($mol/m\ s\ Pa^{0.61}$)	Coefficient of Regression (R^2)
900	0.005348	1.876×10^{-09}	0.9888
1100	0.005611	2.037×10^{-09}	0.9093
1300	0.006267	2.275×10^{-09}	0.9656

It was observed that hydrogen permeation flux through the membrane was directly proportional to the hydrogen partial pressures of the retentate to the power n. The average value of 'n' was 0.61. The possible effects of the internal and external mass transfer in the diffusion mechanism through the membrane may have caused the deviation from 0.5, the common value of 'n'. Also, another reason for the pressure exponent to be different could be the dependence of the permeability constant on the hydrogen concentration.

The membrane permeability constant is proportional to the product of the solubility constant and diffusivity of the hydrogen/palladium system as given in Eq. 3.4. Thus, any changes in either of these values for the hydrogen/palladium system could account for an increase or decrease in permeability. The diffusion coefficient of the palladium-hydrogen system has been shown to increase with increasing partial pressure (54) under sub-atmospheric studies, thereby possibly increasing the membrane permeability. It is likely that the Sievert's constant would also be influenced by higher pressure. It has been postulated that an increased concentration of hydrogen atoms within palladium may form a non-ideal solution in which the dissolved hydrogen atoms would exhibit attractive forces towards one another (37). Such an effect would result in a concentration of

hydrogen atoms greater than that predicted by the Sievert's constant obtained from low-pressure solubility data (52). In this case, the Sievert's constant for hydrogen-palladium would increase with increasing pressure over the range of pressure conditions examined. Thus, the product of the Sievert's constant and the diffusion coefficient of the palladium-hydrogen system may increase with hydrogen pressure, resulting in increase in the membrane permeability. If the permeability, as defined as `k' in Eq. 3.6, is held constant, the net mathematical effect is an increase in the partial pressure exponent with increasing hydrogen pressure. The increase of the exponent value from 0.5 to 0.62 for the high-pressure study may be attributed to an invalid assumption of a diffusion-limited mechanism and/or changes in the Sievert's constant and diffusion coefficient with increasing pressure. An increase in 'n' could also result when the permeation rate is influenced by the leakage of the hydrogen through defects in the Pd layer, transport resistance of the support, and poisoning of the palladium surface. The rate of the hydrogen permeation through the Pd/Al_2O_3 composite membrane could thus be dependent not only on bulk phase hydrogen diffusion but also on more complex transport mechanism involving the surface processes of hydrogen chemisorption, dissolution and diffusion.

An Arrhenius plot for a Pd/Al_2O_3 membrane is shown in Figure 34. The logarithm of the values of hydrogen permeance was plotted against reciprocal temperature. A straight line was fit to the points and from the slope of the straight line, an apparent activation energy of 5.39 (kJ/mol) was estimated. This value is slightly lower than the range of 11.92-20.50 (kJ/mol) reported by Morreale et al. (53) for thicker palladium membranes.

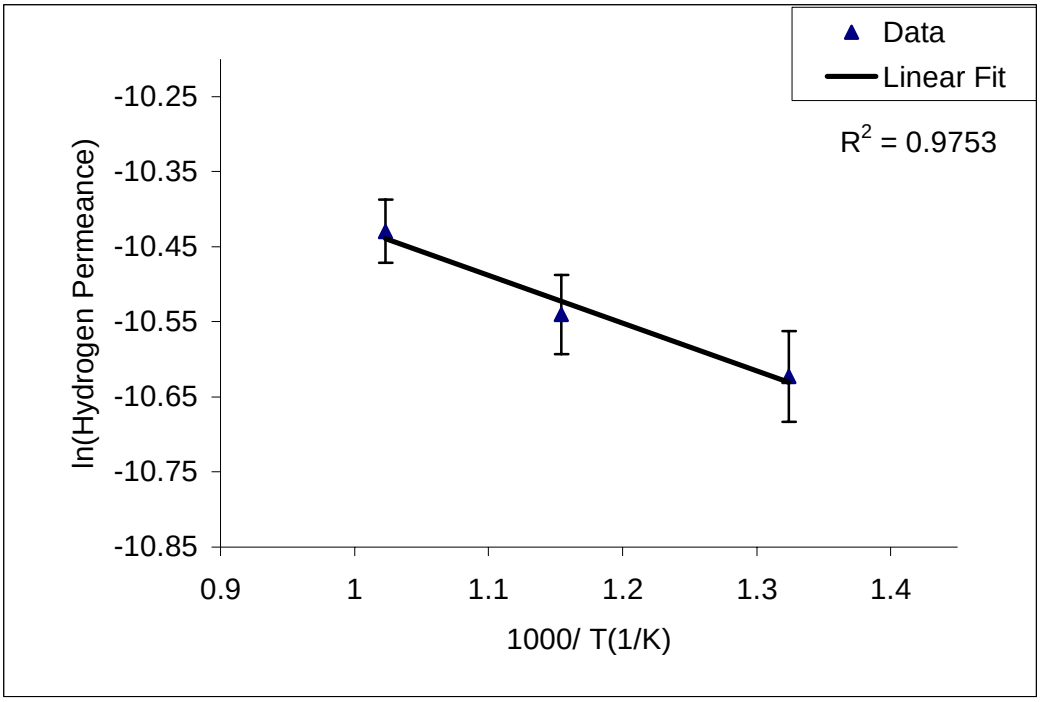

Figure 34 Arrhenius Plot: Logarithm of $\mathscr{P}_{H2}$ vs. 1/T for Pd/Al_2O_3 membrane

However, this value is in the range of earlier reported Pd-Ag membranes, where activation energy has been reported to be in the broader range of 2.2 ~ 23 kJ/mol (48). There is a large spread of activation energies for various membranes. This large variation can probably be explained by the fact that the rate limiting process could vary in different temperature regimes, and with the varying surface composition for different type of membranes. Jayaraman and Lin (56) have suggested that the activation energies will vary between diffusion and surface reaction rate limited membranes. For the hydrogen permeation through a Pd/Al_2O_3 membrane, the apparent activation energy includes the energy barriers for dissolution, diffusion of hydrogen in the Pd layer and for hydrogen permeation in the porous alumina support. Therefore, the activation energies for these membranes with different thicknesses of palladium layers and different supports might be

different. Eventually, the activation energy would increase with increase in mass transfer resistance in the support material. However, the activation energy would not appear to vary with the thickness of Pd dense layer for same support.

Table 7 presents hydrogen permeation fluxes through ceramic supported Pd and Pd-Ag membranes prepared by different methods. The large variation in reported hydrogen permeation flux shows that the flux is a strong function of the method of fabrication of the membrane. The number of layers, average pore sizes and porosities of the ceramic substrates would also affect the permeation fluxes.

The plots of hydrogen permeance flux against partial pressure of hydrogen, at different temperatures, are given in Figure 35-37.

Hydrogen Permeation Results for Platinum Membrane

The platinum membranes fabricated had many pinholes visible to the naked eyes. Thus the permeation tests were not carried out with platinum membranes. The poisoning of pure platinum by CO is also well known. Even trace amounts of CO can be chemisorbed onto the active platinum sites and block the hydrogen dissociation reaction on the platinum surface. So the Pt permeation experiments could not be performed in the simulated syngas environment.

Table 7 Summary of work conducted in the H_2 selective Pd-membrane separation

Method of fabrication	Membrane	Membrane thickness (μm)	Pressure exponent (n)	Flux (mol/m^2)	Activation Energy (kJ/mol)	H_2 Partial pressure difference ΔP_{H2} (kPa)	Temperature (K)	References
CVD	Pd/Al_2O_3	3-5	1	0.102	13-18	100	573	32
Spray pyrolysis	$Pd\text{-}Ag/Al_2O_3$	1.5-2	1	0.08	unknown	≈100	773	35
Electroless plating with osmosis	Pd/Al_2O_3	10	0.65	0.204	12.3	300	645	28
MOVCD	Pd/Al_2O_3	0.5-1	1	0.095	38	400	723	33
MOVCD	Pd/ sol-gel Al_2O_3	0.5-5	1	0.018	30	100	573	57
Electroless plating	Pd/ Al_2O_3	11.4	0.58	0.71	14.45	2445	823	52
Electroless plating	$Pd\text{-}Ag/Al_2O_3$	5.8	≈0.5	0.43	10.7	200	673	29
Electroless plating	Pd/stainless steel	20	0.5	0.091	16.4	300	723	58
Laser	Pd/Al_2O_3	77	0.61	0.061	5.39	380	800	This work

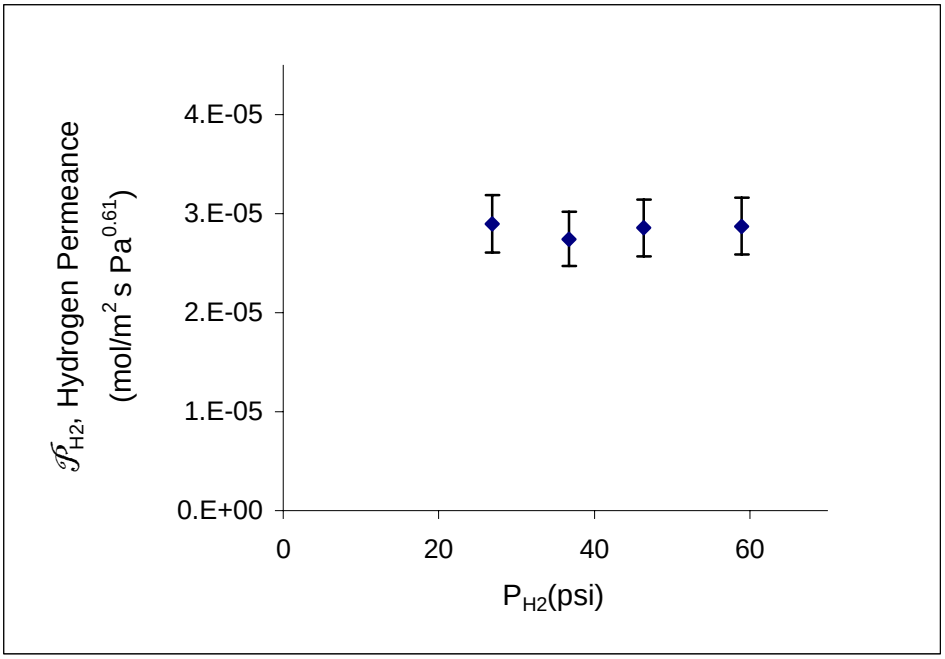

Figure 35 $\mathscr{P}_{H2}$ vs. ΔP_{H2} at 900°F for Pd/Al_2O_3 membrane

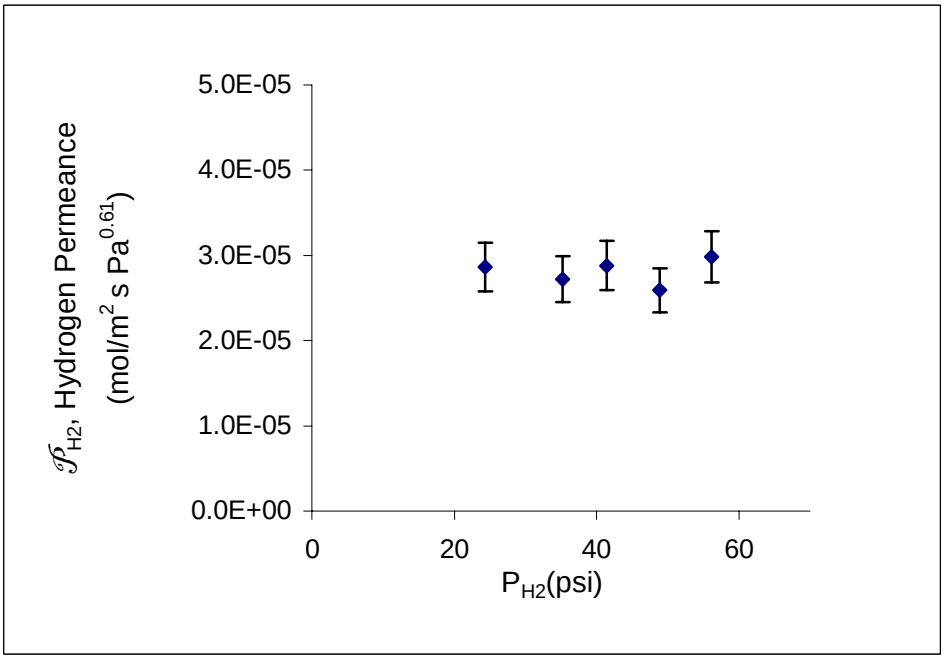

Figure 36 $\mathscr{P}_{H2}$ vs. ΔP_{H2} at 1100°F for Pd/Al_2O_3 membrane

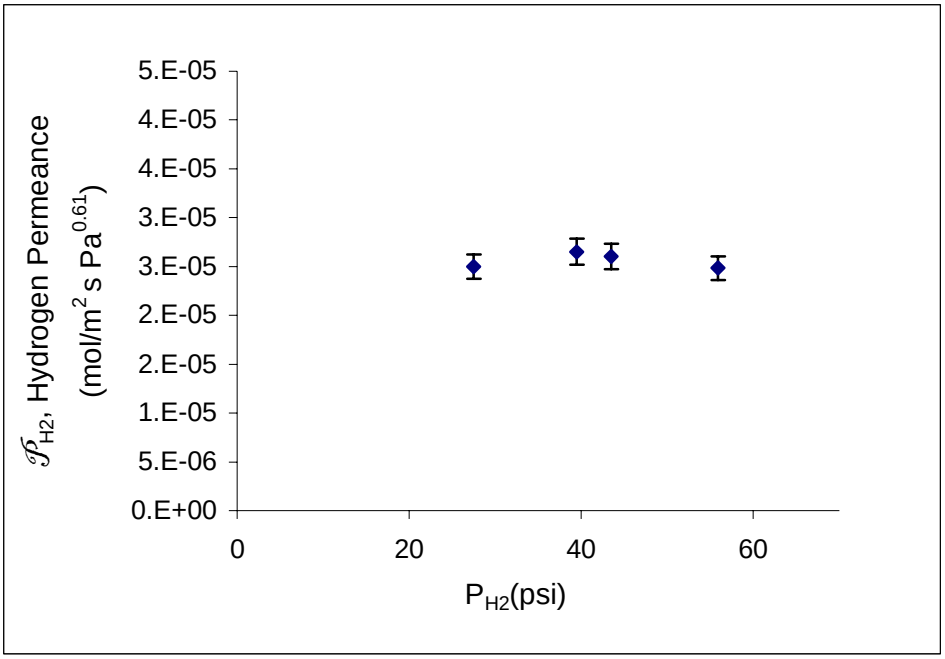

Figure 37 $\mathscr{P}_{H2}$ vs. ΔP_{H2} at 1300°F for Pd/Al_2O_3 membrane

6. CONCLUSIONS AND RECOMMENDATIONS

Conclusions

A study of hydrogen separation from a simulated syngas environment was carried out using a ceramic membrane and in-house prepared ceramic-palladium composite membrane. The hydrogen permeation measurements were carried out in a bench-scale high-pressure, high-temperature reactor system. Experiments were carried out to study the effect of temperature and hydrogen partial pressure on hydrogen permeation. Palladium and Platinum coated ceramic membrane were prepared using UTSI-developed laser-based metal deposition technique and setup called "LISI". Hydrogen permeation flux measurements were also conducted with a commercially-prepared composite membrane supplied by Ceramatec Inc.

Ceramatec® Membrane:

- The membrane provided by Ceramatec Inc. was only permeable to hydrogen. It showed excellent selectivity and no other gas could permeate through it.
- This membrane maintained it selectivity at temperature as high as 1300°F and total pressure as high as 80 psi.
- The hydrogen permeation flux for this membrane was found to be 0.0321 ($mol/m^2.s$) for experiment conducted at 1300°F and at partial pressure of hydrogen of 55 psi.

- The hydrogen permeation flux increased with increasing temperature as well as increasing partial pressure of hydrogen.
- This membrane did not show any decrease in permeance due to any surface poisoning.

Pd and Pt based Membranes:

- A laser-based technique called LISI, was successfully used to deposit thin palladium and platinum films on porous ceramic supports. Although the metallic layers formed were not gas tight, with holes, with more development work on depositing metal precursors on Al_2O_3 substrates and optimizing the laser parameters, gas-tight membranes can be developed.
- This preparation method was found to be faster, less laborious and more efficient in utilizing the metal precursor. Minimizing pinholes in deposited palladium or platinum films, which depends strongly on the use of a defect free alumina membrane support, is the key to ensure a high selectivity of the laser-deposited ceramic-metallic membrane composites.
- The mole fractions of hydrogen on the permeate side corrected for small leakages effects, were used to calculate hydrogen permeation fluxes through the thin metallic film.
- Hydrogen permeation fluxes were measured in the 900-1300°F temperature range and for hydrogen partial pressure upto 55 psi, across the palladium-ceramic membrane. Hydrogen permeation flux of 0.061(mol/m^2 s) was observed at 1300°F and at feed side hydrogen partial pressure of 55 psi.

- The activation energy of the palladium was found to be about 5.39(kJ/mol), in a temperature range of 900-1300°F.
- The hydrogen fluxes of the palladium membrane were almost the double of the Ceramatec® membrane. But with the Ceramatec® membrane, high purity hydrogen separation was possible.
- The Ceramatec® membrane, on the other hand did not have much mechanical strength and was very prone to develop cracks during experiments. The Pd/Al_2O_3 membrane showed enough mechanical strength to withstand gasification conditions.

Recommendations

To continue this research, several areas for further exploration are recommended:

- In hydrogen permeation experiments, volume flow meters should be replaced by mass flowmeters giving a better control of the composition of gases inside the reactor.
- Mass flowmeters will also help in maintaining desired sweep gas flow rates.
- For maintaining constant pressure a back pressure regulator should be used.
- Use of a differential pressure gauge across the membrane will allow more accurate pressure differences to be measured across the membrane, and provide better analyses.
- The Pd and Pt metal membranes formed were not gas tight. More study is needed on the type of precursor and the process of deposition of that precursor on ceramic

substrates. In order to plug all the pinholes, multiple layers of metallic film coatings should be evaluated.

- In Figure 26, the areas of laser-beam overlap during processing created a more even surface. So, the metallic precursor film can be repeatedly treated with the laser-beam. This may plug the holes.
- Coefficients of thermal expansion of Al_2O_3, Pd and CeO_2 are 7.4, 11.52 and 11(10^{-6} K^{-1}), respectively. In this study, alumina was used as the substrate material and the surface layer had coefficient of thermal expansion that expansion is much higher than that of the alumina. In place of alumina, porous ceria discs can be tried as substrates because they have similar coefficient of thermal expansion similar to Pd. This will avoid cracks due to expansion.
- The process of deposition of metallic layers showed technical feasibility of preparing metal-ceramic composite membranes and its possible use in in-situ separation of hydrogen in gasification streams. With encouraging results from this study, using simulated pressure, temperature and gas conditions, actual experiments of hydrogen separation combined with gasification should be performed.

REFERENCES

1. Prabhu, A. K. and Oyama, S. T., “Highly hydrogen selective ceramic membranes: application to the transformation of greenhouse gases,” Journal of Membrane Science, 176, p 233, 2000.
2. Sengupta, A., Sircar, K. K., “Analysis and design of membrane permeators for gas separation,” in R. D. Noble, S. A. Stern (Eds.) Membrane Separation Technology, Principles and Applications, Elsevier, Amsterdam, p 499, 1995.
3. Tsotsis, T. T., Champagnie, A. M., Vasileiadis, S. P., Zraka, Z. D. And Minet, R. G., “Packed bed catalytic membrane reactor,” Chem. Engng Sci. 47, p 2903, 1992.
4. Sun, Y. M. and Khang, S. J., “Catalytic membrane for simultaneous chemical reaction and separation applied to a dehydrogenation reaction,” Ind. Engng Chem. Res, 27, p 1136, 1988.
5. Wu, J. C. S., Gerdes, T. E., Pszczolowski, J. L., Bhave, R. R. and Liu, P. K. T., “Dehydrogeneration of ethylbenzene to styrene using commercial ceramic membranes as reactors,” Separ. Sci. Technol,. 25, p 1489, 1990.
6. Itoh, N., Xu, W.C. and Sathe, A. M., “Capability of permeate hydrogen through palladium-based membranes for acetylene hydrogenation,” Ind. Engng Chem. Res., 32, p 2614, 1993.
7. Uemiya, S., Sato, N., Ando, H. and Kikuchi, E., “The water gas shift reaction assisted by a palladium membrane reactor,” Ind. Engng Chem. Res., 30, p 585, 1991.
8. Gryaznov, V. M. and Slin’ko, M. G., “Selectivity in catalysis by hydrogen-porous membranes, Discuss, Faraday Soc., p 73, 1982.
9. Gryaznov, V. M., Vedernikov, V. I., Gul’yanova, S. G., Kinet, Katal, 27,p 42, 1986.

10. Kamayema, T., Dokiya, M., Fujishige, M., Yokokawa, H. and Fukuda, K., "Possibility for effective production of hydrogen from hydrogen sulfide by means of a porous Vycor glass membrane," Ind. Chem. Fundam., 20, p 297, 1981.
11. Kamayema, T., Fukuda, K., Fujishige, M., Yokokawa, H. and Dokiya, M., "Production of hydrogen from hydrogen sulfide by means of selective diffusion membranes," Adv. Hydrogen Energy Proc., 2, p 569, 1981.
12. Sun, Y.M., Khang, S.J., "Catalytic membrane for simultaneous chemical reaction and separation applied to a dehydrogenation reaction," Ind. Eng. Chem. Res., 27, p 1136, 1988.
13. Itoh, N., "A membrane reactor using palladium," *AIChE J*., 33, p 1576, 1987.
14. Shinji, O., Misono, M., Yoneda, Y., "The dehydrogenation of cyclohexane by the use of a porous-glass reactor," Bull. Chem. Soc., Japan 55, p 2760, 1982.
15. Zaspalis, V. T., van Praag, W., Kiezer, K., van Ommen, J. G., Ross, J. R. H., and Burggraaf, A. J., "Reactor studies using alumina separation membranes for the dehydrogenation of methanol and *n*-butane," Appl. Catal., 74, p 223, 1991.
16. Chai, M., Machida, M., Eguchi, K. and Arai, H., "Promotion of hydrogen permeation on metal-dispersed alumina membranes and its application to a membrane reactor for methane steam reforming," Appl. Catal. A. Gen., 110, p 239, 1994.
17. Tsotsis, T. T., Champagnie, A. M., Vasileiadis, S. P., Ziaka, Z. D. and Minet, R. G., "The enhancement of reaction yield through the use of high temperature membrane reactors," Sep. Sci. Technol., 28, p 397, 1993.

18. Marcano, J.G.S., Tsotsis,T. T., "Catalytic Membranes and Membrane Reactors," Wiley-VCH Verlag GmbH, Weinheim, 2002.
19. Van Der Berg, G.B., and Smolders, C.A., "Diffusional phenomena in membrane separation processes," J. Membr. Sci., 73,p 103, 1992.
20. Gavalas, G.R., Soojin, K., "Preparation of H_2 Permselective Silica Membranes by Alternating Reactant Vapor Deposition," Ind. Eng. Chem. Res., 34, p168, 1995.
21. Kitao, S., Asaeda, M., "Gas separation performance of thin porous silica membrane prepared by sol-gel and CVD methods," Key Eng. Mater. , 61(6), p 267, 1991.
22. Sea, B.K., Wantanabe, M., Kusakabe, K., and Morooka, S., "Formation of hydrogen permselective silica membrane for elevated hydrogen recovery from a mixture containing steam," Gas Sep. Purif. 10, p 187, 1996.
23. Perry, R.H., Green, D.W., "Perry's Chemical Engineers' Handbook," 7th Edition, p 22, 1997.
24. Egan, B. Z., Fain, D.E., Roettger, G.E., White, D. E., "Separating hydrogen from coal gasification gases with alumina membranes," Journal of Engineering for Gas Turbines and Power, Transactions of the ASME, 114, p 367-370, April 1992.
25. Kono, M., Shindo, M., S. Sugawara, and S. Sato, "A composite palladium and porous aluminum oxide membrane for hydrogen gas separation," J. Chem, Sci., 37, p 193, 1988.
26. F.A. Lewis, "The Palladium Hydrogen System," Academic Press, London, 1967.
27. Buxbaum, R.E., Marker, T.L., "Hydrogen transport through non-porous membranes of palladium-coated niobium, tantalum and vanadium," J. Membrane Sci., 85, p 29, 1993.

28. Li, A., Liang, W., Hughes. R., " Fabrication of defect-free Pd/α-Al2O3 composite membranes for hydrogen separation," Thin Solid Films 350, p106,1999
29. Uemiya, S., Matsuda, T., Kikuchi, E., "Hydrogen permeable palladium-silver alloy membrane supported on porous ceramics," J. Membrane Sci., 56, p 315, 1991.
30. Konno, M., Shindo, M., Sugawara, S., and Sato, S., "A composite palladium and porous aluminum oxide membrane for hydrogen gas separation," J. Membrane Sci., 37, p 193, 1998.
31. Shu, J., Grandjean, B.P.A., Ghali, E., and Kaliaguine, S., " Simultaneous deposition of Pd and Ag on porous stainless steel by electroless plating," J. Membrane Sci., 77 ,p 181, 1993.
32. Yan, S., Maeda, H., Kusakabe, K., and Morooka, S., "Thin palladium films formed in support pores by metal-organic chemical vapor deposition method and application to hydrogen separation," Ind. Eng. Chem. Res., 33, p 616, 1994.
33. Lin, Y.S., Xomeritakis, G., "Fabrication of a thin palladium membrane supported in a porous ceramic substrate by chemical vapor deposition," Journal of Membrane Science, 120, p 261, 1996.
34. Feurer, E., and Suhr, H., "Thin palladium films prepared by metal organic plasma enhanced CVD," Thin Solid Films, 157, p 81, 1988.
35. Li, Z.Y., Maeda, H., Kusakabe, K., Morooka, S., Anzai, H., and Akiyama, S., "Preparation of palladium-silver alloy membranes for hydrogen separation by the spray pyrolysis method," J. Membrane Sci., 78, p 247, 1993.
36. Dahotre, N. B., Semak, V., Xiao, C., McCay, M.H., "Non-vacuum laser deposition of buffer layers for coated conductors," Journal of Thin Solid Films, 340, p 77, 1999.

37. Buxbaum, R.E., and Kinney, A.B., "Hydrogen transport through tubular membranes of palladium-coated tantalum and niobium," Ind. Eng. Chem. Res., 35, p 530, 1996.
38. Agarwal, A., "Laser surface engineering of composite titanium diboride coating on steel: synthesis and characterization," Ph.D Dissertation-University of Tennessee,p 6, 1999.
39. Agarwal, A., Katipelli, L. R., Dahotre, N. B., "Elevated temperature oxidation of laser surface engineered composite boride coating on steel," Metallurgical and materials transactions, 31A, p 461, 2000.
40. Agarwal, A., Katipelli, L. R., Dahotre, N. B., "Laser surface engineered TiC coating on 6061 Al alloy Microstructure and wear," Applied surface science, 153, p 65, 2000.
41. Kadolakar, P., Dahotre, N. B., "Variation of structure with input energy during laser surface engineering of ceramic coatings on aluminum alloys," Applied Surface science, 199, p 222, 2002.
42. Khangar, A., Kenik, E. A., Dahotre, N. B., "Microstructure and microtexture in laser-dressed alumina grinding wheel material," Ceramic International, 31, p 621, 2005.
43. Jackson, M. J., Robinson, G. M., Dahotre, N. B., "Laser dressing of alumina grinding wheels," Heat Treating and Surface Engineering Congress & Exposition 2003, ASM International, Materials Park, OH, p 423, 2003.
44. Dahotre, N. B., "Laser Surface engineering." Advanced materials & processes, p 35, July 2002.

45. Collot, A.G., "Getting hydrogen from coal: effort is being made to develop membranes to separate the hydrogen from coal syngas," Energy, v29 i4, p38, 2004.
46. Elangovan, S., Nair, B., Small, B. H., Timper, M., Hartvgisen, J., Wilson, M., "Ceramic membrane devices for ultra-high purity hydrogen production," Presented at the American Chemical Society, Advances in membrane for energy and fuel application, Symposium, Macrh 23-27, 2003.
47. Chang, C.H., Gopalan, R., and Lin, Y.S., "Thermal and hydrothermal stability study of alumina, titania and zirconia ceramic membranes," J. Membrane Sci., 91, p 27-45, 1993.
48. Yoldas, B.E., "Alumina sol preparation from alkoxides," Ceramic Bulletin, 54,p 289, 1975.
49. Qi, X., Lin, Y. S., "Electrical conduction and hydrogen permeation through mixed proton–electron conducting strontium cerate membranes,"Solid State Ionics, 130, i1-2, p 149-156, 2000.
50. Siriwardane, R.V., Poston, J.A., Fisher, E.P., Lee, T.H., Dorris, S.E., Balachandran, U., "Characterization of ceramic-metal composite hydrogen separation membranes consisting of barium oxide, cerium oxide, yttrium oxide and palladium," Applied Surface Science, 217, p 43, 2003.
51. Guan, J., Dorris, S.E., Balachandran, U., Liu, M., "Transport properties of $SrCe_{0.95}Y_{0.05}O_{3-\delta}$ and its application for hydrogen separation," Solid State Ionics 110, p 303, 1998.
52. Collins, J.P., and Way, J.D., "Preparation and characterization of a composite palladium- ceramic membrane," Ind. Eng. Chem. Res., 32, p 3006, 1993.

53. Morreale, B. D., Ciocco, M.V., Enick , R. M , Morsi , B. I. ,Howarda, B. H., Cugini , A.V. , Rothenberger, K. S., "The permeability of hydrogen in bulk palladium at elevated temperatures and pressures," J. Membrane Sci, 212, p 87, 2003.
54. Holleck, G .L., "Diffusion and solubility of hydrogen in palladium and palladium-silver alloys," J. Phys . Chem., 74 (3), p503, 1970.
55. Amandusson, H., Ekedahl, L.G., Dannetun, H., "Hydrogen permeation through surface modified Pd and PdAg membranes," Journal of Membrane Science, 193, p 35, 2001.
56. Jayaraman, V., Lin, Y.S., "Syntesis and hydrogen permeation of ultrathin palladium-silver alloy membranes," J. Membrane Sci, 104, p 251, 1995.
57. Xomeritakis, G., Lin, Y.S., "CVD synthesis and gas permeation properties of thin palladium/alumina membranes," AIChE J., 44, p 174, 1998.
58. Mardilovich, P.P., She, Y., Ma, Y.B., Rei, M.H., "Defect-free palladium membranes on porous stainless-steel support," AIChE J., 44, p 320, 1998.

APPENDICES

Appendix I-Data for Palladium Membrane

Table 8 Permeate side data for Pd membrane

Run #	Peak Areas					$T_{Reactor}$ (°F)	$P_{Reactor}$ (psi)	Time for 20 cc of gas to flow	
	H_2	N_2	CH_4	CO	CO_2			t_1(s)	t_2(s)
1	2003.94	1519.30	20.06	0.00	8.42	700	40	4.87	4.97
2	5585.96	1050.51	77.00	52.10	92.66	1100	40	4.65	4.6
3	5644.60	1056.14	75.02	51.22	94.72	1100	60	3.6	3.58
4	7055.79	860.20	111.21	65.91	134.57	1100	80	3.71	3.58
5	6727.69	885.17	133.26	93.93	105.69	900	80	4.72	4.43
6	983.00	1587.80	8.01	0.00	0.00	900	60	3.42	3.51
7	1796.05	1510.69	17.89	2.73	3.79	900	40	4.87	4.91
8	1411.51	1555.90	13.90	0.00	1.32	1300	40	3.31	3.18
9	951.20	1624.71	3.00	0.00	1.26	1300	60	3.52	3.6
10	2860.80	1468.98	25.55	14.38	7.85	1300	80	4.68	4.59
11	4113.24	1202.54	62.27	46.01	42.55	900	40	4.8	4.2
12	4105.13	1184.04	81.21	55.77	50.92	900	60	4.13	4.06
13	9180.29	513.11	227.25	200.68	143.24	900	80	3.45	3.41
14	5974.74	1003.42	90.19	96.18	43.03	1300	40	3.74	3.84
15	4747.97	835.02	204.66	186.36	109.27	1300	60	3.65	3.61
16	1402.48	1544.23	8.28	2.53	4.77	1100	40	6.83	7.93
17	1810.87	1442.37	22.27	8.87	14.99	1100	60	4.02	7.82
18	1660.07	1524.33	12.61	6.99	15.20	1100	80	4.41	6.28

Table 9 Feed side data for Pd membrane

Run#	Peak Areas				$T_{Reactor}$(°F)	$P_{Reactor}$(psi)
	H_2	CH_4	CO	CO_2		
1	12152.29	156.83	154.97	288.16	700	40
2	12427.81	197.79	166.13	281.24	1100	40
3	12359.81	186.87	155.94	263.87	1100	60
4	12355.65	190.34	156.98	269.41	1100	80
5	11951.30	233.77	212.74	219.30	900	80
6	11527.71	180.17	174.63	185.22	900	60
7	11349.18	164.23	214.03	194.85	900	40
8	11099.96	168.38	255.99	155.33	1300	40
9	12034.96	154.35	214.93	133.77	1300	60
10	12302.24	179.27	230.24	141.94	1300	80
11	12626.82	228.55	226.83	181.04	900	40
12	11636.09	273.77	237.21	206.01	900	60
13	11458.11	308.38	237.56	219.52	900	80
14	12632.88	211.99	253.45	148.34	1300	40
15	11870.25	228.48	302.34	179.74	1300	60
16	12765.14	276.36	195.85	227.72	1100	40
17	12218.41	289.61	171.89	240.36	1100	60
18	12542.92	268.91	160.11	230.60	1100	80

Table 10 Data for permeate side calibration gases for Pd membrane

Run#	Peak Areas				
	H_2	N_2	CH_4	CO	CO_2
1	17057.17	1759.171	5765.15	1688.526	1590.015
2	17057.17	1759.171	5765.15	1688.526	1590.015
3	17057.17	1759.171	5765.15	1688.526	1590.015
4	17057.17	1759.171	5765.15	1688.526	1590.015
5	17057.17	1759.171	5765.15	1688.526	1590.015
6	17057.17	1759.171	5765.15	1688.526	1590.015
7	17057.17	1759.171	5765.15	1688.526	1590.015
8	17057.17	1759.171	5765.15	1688.526	1590.015
9	17057.17	1759.171	5765.15	1688.526	1590.015
10	17057.17	1759.171	5765.15	1688.526	1590.015
11	16785.72	1670.388	6218.83	1682.023	1562.031
12	16785.72	1670.388	6218.83	1682.023	1562.031
13	16785.72	1670.388	6218.83	1682.023	1562.031
14	16785.72	1670.388	6218.83	1682.023	1562.031
15	16785.72	1670.388	6218.83	1682.023	1562.031
16	17785.78	1577.338	5983.12	1724.646	1506.451
17	17785.78	1577.338	5983.12	1724.646	1506.451
18	17785.78	1577.338	5983.12	1724.646	1506.451

Table 11 Data for feed side calibration gases for Pd membrane

Run#	Peak Areas				
	H_2	N_2	CH_4	CO	CO_2
1	17057.17	1759	5765.15	1688.526	1590.015
2	17057.17	1759	5765.15	1688.526	1590.015
3	17057.17	1759	5765.15	1688.526	1590.015
4	17057.17	1759	5765.15	1688.526	1590.015
5	17057.17	1759	5765.15	1688.526	1590.015
6	17057.17	1759	5765.15	1688.526	1590.015
7	17057.17	1759	5765.15	1688.526	1590.015
8	17057.17	1759	5765.15	1688.526	1590.015
9	17057.17	1759	5765.15	1688.526	1590.015
10	17057.17	1759	5765.15	1688.526	1590.015
11	16785.72	1670	6218.83	1682.023	1562.031
12	16785.72	1670	6218.83	1682.023	1562.031
13	16785.72	1670	6218.83	1682.023	1562.031
14	16785.72	1670	6218.83	1682.023	1562.031
15	16785.72	1670	6218.83	1682.023	1562.031
16	17785.78	1577	5983.12	1724.646	1506.451
17	17785.78	1577	5983.12	1724.646	1506.451
18	17785.78	1577	5983.12	1724.646	1506.451

Appendix II-Data for Ceramatec® membrane

Table 12 Permeate side data for Ceramatec® membrane

Run#	H_2	N_2	$T_{Reactor}$(°F)	$P_{Reactor}$(psi)	Time for 20 cc of gas to flow	
					t_1(s)	t_2(s)
1	48.08	1675.53	500	40	4.85	4.82
2	34.09	1616.11	700	40	4.97	4.86
3	39.92	1623.12	900	40	4.70	4.83
4	98.75	1609.48	900	40	4.87	4.83
5	81.25	1474.97	1100	40	4.78	4.86
6	116.15	1669.62	1100	60	3.47	3.48
7	92.89	1671.99	1100	80	4.93	4.90
8	145.17	1708.79	1100	80	4.93	4.90
9	159.83	1680.79	1100	80	3.04	3.01
10	183.84	1707.93	1300	80	3.04	3.05
11	340.47	1724.38	1300	40	4.11	4.30
12	339.76	1708.40	1300	60	3.52	3.62
13	458.00	1655.39	1300	80	4.35	4.20
14	450.83	1675.42	1300	80	4.28	4.26
15	337.36	1722.43	500	60	5.60	7.10
16	111.31	1690.48	500	60	5.32	5.35
17	92.44	1669.74	500	80	3.60	3.50
18	215.97	1719.66	700	80	3.65	3.66
19	196.19	1710.60	700	80	3.65	3.66
20	511.99	1722.92	1100	60	5.97	3.97
21	441.45	1674.23	1100	60	4.09	4.08
22	675.15	1648.87	1100	80	4.26	4.27
23	659.36	1643.84	1100	80	4.26	4.26
24	29.92	1676.99	70	30	6.77	7.14
25	29.80	1708.24	70	30	6.90	7.04
26	47.40	1689.25	70	40	8.71	8.72
27	20.33	1669.69	70	60	3.32	3.28
28	15.01	1580.69	70	50	3.90	3.90
29	17.49	1679.91	70	50	4.01	3.91
30	20.73	1772.73	70	60	3.30	3.28
31	43.56	1634.23	70	40	8.60	8.54
32	25.46	1687.18	70	70	4.91	4.86
33	36.22	1673.85	70	80	6.05	6.11
34	29.21	1684.09	70	70	4.94	4.80
35	19.89	1677.50	70	60	3.33	3.35
36	41.90	1688.74	70	80	6.02	6.11

Table 13 Feed Side data for Ceramatec® membrane

Run#	Peak Areas				$T_{Reactor}$(°F)	$P_{Reactor}$(psi)
	H_2	CH_4	CO	CO_2		
1	10492.56	233.98	325.58	380.30	500	40
2	10217.71	251.61	242.14	407.28	700	40
3	5709.78	413.28	452.59	576.64	900	40
4	10258.88	264.02	258.21	312.63	900	40
5	11094.45	269.31	338.04	244.54	1100	40
6	9790.06	294.72	357.49	316.97	1100	60
7	7935.18	363.51	489.55	423.84	1100	80
8	7929.22	361.11	488.14	418.34	1100	80
9	11681.69	259.76	249.22	244.19	1100	80
10	11886.62	223.95	297.43	175.72	1300	80
11	11899.32	195.92	307.15	169.27	1300	40
12	12357.35	188.72	249.09	216.05	1300	60
13	11518.20	207.60	316.10	172.47	1300	80
14	11523.12	208.61	314.90	171.89	1300	80
15	12845.93	123.57	113.12	202.07	500	60
16	12459.28	144.59	188.91	245.66	500	60
17	11667.73	147.28	166.97	245.25	500	80
18	12098.30	156.07	139.44	240.43	700	80
19	12088.51	154.04	141.20	239.84	700	80
20	12673.92	188.37	195.63	163.17	1100	60
21	11945.18	213.97	233.08	208.42	1100	60
22	11573.96	236.82	234.46	235.15	1100	80
23	11573.96	236.82	234.46	235.15	1100	80
24	12356.71	172.87	177.19	289.72	30	70
25	12356.71	172.87	177.19	289.72	30	70
26	12562.39	160.91	319.16	270.05	40	70
27	12570.75	164.55	162.14	283.64	60	70
28	13712.94	134.28	148.10	262.33	50	70
29	13712.94	134.28	148.10	262.33	50	70
30	12570.75	164.55	162.14	283.64	60	70
31	12508.69	151.90	158.42	247.30	40	70
32	12337.05	166.29	201.90	280.98	70	70
33	12502.06	153.14	150.28	286.99	80	70
34	12620.52	165.92	156.20	281.21	70	70
35	12570.75	164.55	162.14	283.64	60	70
36	6974.60	146.28	230.18	250.48	80	70

Table 14 Data for permeate side calibration gases for Ceramatec® membrane

Run#	Peak Areas	
	H_2	N_2
1	16381.18	1754.111
2	16381.18	1754.111
3	16381.18	1754.111
4	16381.18	1754.111
5	16381.18	1754.111
6	16381.18	1754.111
7	16381.18	1754.111
8	16381.18	1754.111
9	16381.18	1754.111
10	16381.18	1754.111
11	16381.18	1754.111
12	16381.18	1754.111
13	16161.6	1754.111
14	16161.6	1754.111
15	17056.85	1754.111
16	17056.85	1754.111
17	17056.85	1754.111
18	17056.85	1754.111
19	17056.85	1754.111
20	16161.6	1754.111
21	16161.6	1754.111
22	16161.6	1754.111
23	16161.6	1754.111
24	17041.9	1782.408
25	17041.9	1782.408
26	17041.9	1782.408
27	16018.47	1782.408
28	16018.47	1782.408
29	16018.47	1782.408
30	16018.47	1782.408
31	16018.47	1782.408
32	16018.47	1782.408
33	16018.47	1782.408
34	16018.47	1782.408
35	16018.47	1782.408
36	16018.47	1782.408

Table 15 Data for feed side calibration gases for Ceramatec® membrane

Run#	Peak Areas				
	H_2	N_2	CH_4	CO	CO_2
1	17380.21	1754.111	5549.84	1660.389	1510.076
2	17380.21	1754.111	5549.84	1660.389	1510.076
3	17380.21	1754.111	5549.84	1660.389	1510.076
4	17380.21	1754.111	5549.84	1660.389	1510.076
5	17380.21	1754.111	5549.84	1660.389	1510.076
6	17380.21	1754.111	5549.84	1660.389	1510.076
7	17380.21	1754.111	5549.84	1660.389	1510.076
8	17380.21	1754.111	5549.84	1660.389	1510.076
9	17380.21	1754.111	5549.84	1660.389	1510.076
10	17380.21	1754.111	5549.84	1660.389	1510.076
11	17380.21	1754.111	5549.84	1660.389	1510.076
12	17380.21	1754.111	5549.84	1660.389	1510.076
13	17380.21	1754.111	5549.84	1660.389	1510.076
14	17380.21	1754.111	5549.84	1660.389	1510.076
15	17380.21	1754.111	5549.84	1660.389	1510.076
16	16161.6	1754.111	5549.84	1660.389	1510.076
17	17380.21	1754.111	5549.84	1660.389	1510.076
18	17056.85	1754.111	5916.6	1568.7	1697.075
19	17056.85	1754.111	5916.6	1568.7	1697.075
20	16161.6	1754.111	5549.84	1660.389	1510.076
21	16161.6	1754.111	5549.84	1660.389	1510.076
22	16161.6	1754.111	5549.84	1660.389	1510.076
23	16161.6	1754.111	5549.84	1660.389	1510.076
24	16018.47	1782.408	5944.86	1721.663	1455.142
25	16018.47	1782.408	5944.86	1721.663	1455.142
26	16350.86	1782.408	5810.98	1673.317	2050.098
27	16350.86	1782.408	5810.98	1673.317	2050.098
28	16018.47	1782.408	5944.86	1721.663	1455.142
29	16018.47	1782.408	5944.86	1721.663	1455.142
30	16350.86	1782.408	5810.98	1673.317	2050.098
31	16018.47	1782.408	5944.86	1721.663	1455.142
32	16018.47	1782.408	5944.86	1721.663	1455.142
33	16018.47	1782.408	5944.86	1721.663	1455.142
34	16018.47	1782.408	5944.86	1721.663	1455.142
35	16350.86	1782.408	5810.98	1673.317	2050.098
36	16018.47	1782.408	5944.86	1721.663	1455.142

Appendix III-Sample Calculation for Run#16 of Pd-Membrane

Area under Gas Chromatograph peaks

Run16	H_2	N_2	CH_4	CO	CO_2
Feed	12765.14	0	276.357	195.851	227.715
Permeate	1402.48	1544.225	8.284	2.528	4.768
Calibration	17785.78	1577.338	5983.12	1724.646	1506.451

Mole Fractions of Gases

Run16	H_2	N_2	CH_4	CO	CO_2
Feed	0.717716	0	0.046189	0.11356	0.15116
Permeate	0.078854	0.979007	0.001385	0.001466	0.003165

Corrected Mole Fractions on basis of Methane

Run16	H_2	N_2	CH_4	CO	CO_2
Feed	0.717716	0	0.046189	0.161663	0.254042
Permeate	0.078854	0.979007	0.001385	0.001466	0.003165

Normalized Mole fractions

Run16	H_2	N_2	CH_4	CO	CO_2
Feed	0.608435	0	0.039157	0.137048	0.215361
Permeate	0.073578	0.913503	0.001292	0.004522	0.007106

Volumetric Flow rate of permeate side sample gases

t_1(s)	t_2(s)	Vol. of Flow (cc)	Flow rate (cc/s)	Flow rate(cc/min)
6.83	7.93	20	2.71	162.60

Effective area of membrane=$\pi \times (1.4)^2 = 1.539379$ cm^2

$$J_{Total} = 0.07358 \times \left(\frac{162.6}{1.539379} \right) = 7.771 \text{ (cc/cm}^2 \text{ min)}$$

$$J_{pinhole} = \left(\frac{0.608435}{0.039157} \times 0.001292 \right) \times \left(\frac{162.60}{1.539379} \right) = 2.1205 \text{(cc/cm}^2 \text{ min)}$$

$$J_{metal} = J_{Total} - J_{pinholes}$$

$$J_{metal} = (7.771 - 2.121) \text{(cc/cm}^2 \text{ min)}$$

$$J_{metal} = 5.65 \text{(cc/cm}^2 \text{ min)}$$

Appendix IV-Variation of Equilibrium Constant with Pressure

$$H_2 \rightleftarrows 2H$$

$$K_P = \frac{P_H^2}{P_{H_2}}$$

$$K_P = \frac{(2y_{H_2}P)^2}{(1-y_{H_2})P}$$

$$K_P = \frac{4y_{H_2}{}^2P}{(1-y_{H_2})}$$

K_P is equilibrium constant and P is the total pressure.

VITA

Binay Kumar Singh was born in Bihar, India on April 13, 1978. He received his undergraduate degree in Chemical Engineering from the Indian Institute of Technology, Roorkee, India in June 2001. From July 2001 to July 2003 he worked as an Assistant system Engineer in Tata Consultancy Service, India. In August 2003 he joined the University of Tennessee Space Institute as Graduate Research Assistant to pursue Master of Science degree in Chemical Engineering.

He plans to Rensselaer Polytechnic Institute, NY, in the fall 2005 to pursue his PhD in Chemical Engineering.